Diagnosing uncertainties in global biomass burning emission inventories and their impact on modeled air pollutants

Wenxuan Hua[1,2,] Sijia Lou[1,2,3*], Xin Huang[1,2,3], Lian Xue[1,2,3], Ke Ding[1,2,3] Zilin Wang[1,2], Aijun Ding[1,2,3]

[1] Joint International Research Laboratory of Atmospheric and Earth System Sciences, School of Atmospheric Sciences, Nanjing University, Nanjing 210023, China.

[2] Jiangsu Provincial Collaborative Innovation Center for Climate Change, Nanjing, China.

[3] Frontiers Science Center for Critical Earth Material Cycling, Nanjing University, Nanjing, China.

Corresponding author: Sijia Lou (lousijia@nju.edu.cn)

Abstract

Large uncertainties persist within current Biomass burning (BB) inventories, and the choice of these inventories can substantially impact model results when assessing the influence of BB aerosols on weather and climate. We evaluated discrepancies among BB emission inventories by comparing carbon monoxide (CO) and organic carbon (OC) emissions from seven major BB regions globally between 2013 and 2016. Mainstream bottom-up inventories, including Fire INventory from NCAR 1.5 (FINN1.5) and Global Fire Emissions Database version 4s (GFED4s), along with top-down inventories Quick Fire Emissions Dataset 2.5 (QFED2.5) and VIIRS-based Fire Emission Inventory version 0 (VFEI0), were selected for this study.

Global CO emissions range from 252 to 336 Tg, with regional disparities reaching up to a sixfold difference. Dry matter is the primary contributor to the regional variation in CO emissions (50-80%), with emission factors accounting for the remaining 20-50%. Uncertainties in dry matter often arise from biases in calculating bottom fuel consumption and burned area, influenced by vegetation classification methods and fire detection products. In the tropics, peatlands contribute more fuel loads and higher emission factors than grasslands. At high latitudes, increased cloud fraction amplifies the discrepancy in estimated burned area (or fire radiative power) by 20%. The global OC emissions range from 14.9 to 42.9 Tg, exhibiting higher variability than CO emissions due to the corrected emission factors in QFED2.5, with regional disparities reaching a factor of 8.7.

Additionally, we applied these BB emission inventories to the Community Atmosphere Model version 6 (CAM6) and assessed the model performance against observations. Our results suggest that the simulations based on the GFED4s agree best with the MOPITT-retrieved CO. While comparing the simulation with Moderate Resolution Imaging Spectroradiometer (MODIS) and AErosol RObotic NETwork (AERONET) aerosol optical depth (AOD), our results reveal that there is no global optimal choice for BB inventories. In the high latitudes of the Northern Hemisphere, using GFED4s and QFED2.5 can better capture the AOD magnitude and diurnal variation. In equatorial Asia, GFED4s outperform others in representing day-to-day changes, particularly during intense burning. In Southeast Asia, we recommend using the OC emission magnitude from FINN1.5 combined with daily variability from QFED2.5. In the Southern Hemisphere, the latest VFEI0 has performed relatively well. This study has implications for reducing the uncertainties in emissions or improving BB emission inventories in further studies.

1 Introduction

In recent years, extreme wildfire events have occurred frequently around the world (Balshi et al., 2009; Knorr et al., 2016; Yang et al., 2019; Junghenn Noyes et al., 2022). The size of the fire has consistently broken records over the last decades (Westerling et al., 2006; Westerling and Bryant, 2008; Brando et al., 2020), threatened lives and infrastructure, and continuously jeopardized the global economy. Wildfires are also one of the most important sources of biomass burning (BB) emissions, which can emit loads of gaseous and particulate pollutants (Ferek et al., 1998; Adams et al., 2019), detrimental to regional air quality and human health (Reid et al., 2005, Reid and Mooney, 2016). Additionally, BB aerosols, predominantly black carbon (BC) and organic carbon (OC) can affect regional climate by absorbing/scattering solar radiation, acting as cloud condensation nuclei, and altering cloud albedo (Spracklen et al., 2011; Boucher et al. 2013). Recent studies have shown that aerosols produced by biomass burning can significantly affect changes in temperature, cloud fraction, precipitation, and even the circulation structure (Christian et al., 2019; Yang et al., 2019; Yu et al., 2019; Carter et al., 2020; Jiang et al.,2020; Ding et al., 2021; Huang et al., 2023). However, these changes in meteorology are sensitive to the choice of BB emission inventory.

Previous studies often found that there is a significant deviation between the gaseous or particulate pollutants simulated by the model and the satellite retrieval value (Bian et al., 2007; Chen et al., 2009; Carter et al., 2020), one of the most important reasons comes from the uncertainties in emission inventories. For example, Bian et al. (2007) applied six different BB emission inventories, GFED1 and GFED2 (Global Fire Emissions Database version 1 and 2) (GFED1 and GFED2), Arellano1, Arellano2, Duncan1, and Duncan2, to the Unified Chemistry Transport Model (UCTM). They reported that although the total global CO of the six BB emission inventories was within 30% of each other, the model results suggested that regional deviations can be much higher, by as much as 2-5 times, especially in the Southern Hemisphere. Bias in emission inventories can therefore often have a significant impact on the direct and indirect effects of models on aerosol assessments (Liu et al., 2018; Liu et al., 2020a; Ramnarine et al., 2019; Carter et al., 2020). Carter et al. (2020) compared the simulated black carbon (BC) and organic carbon (OC) concentrations with measurements from IMPROVE (Interagency Monitoring of Protected Visual Environments) observation network from May to September. They suggested that using the FINN1.5 inventory (Fire INventory from NCAR 1.5) improves model results in eastern North America, while using GFED4s, QFED2.4 (Quick Fire Emissions Dataset 2.4), and GFAS1.2 (Global Fire Assimilation System 1.2) inventories shows better agreement with observations in western North America. They also noted that population-weighted BB $PM_{2.5}$ concentrations in Canada and the adjacent United States could vary between 0.5 and 1.6 $\mu g\ m^{-3}$ in 2012 by using different BB emissions. Liu et al. (2018) used the global model CAM5 (The Community Atmosphere Model 5) and three different BB emission inventories to analyze the uncertainties in the aerosol radiative effects in the Northeastern United States in early April 2009. They found that aerosols exhibited a stronger cooling effect when CAM5 used the QFED2.4 inventory than the GFED3.1 and GFED4s inventories, with additional cooling of -0.7 W m^{-2} and -1.2 W m^{-2} through aerosol direct radiative effect and the aerosol-cloud radiative effect, respectively. On a global basis, Ramnarine et al. (2019) used the global model GEOS-Chem-TOMAS (GEOS-Chem-TwO-Moment Aerosol Sectional), and found that the direct radiative effects and indirect effects of aerosols driven by the FINN1.5 emission inventory in 2010 were 70% and 10% lower than those driven by GFED4, respectively. Therefore,

to better estimate regional aerosol-radiation/aerosol-cloud interactions in wildfire regions, it is necessary to understand the differences in emission inventories from biomass combustion and the main drivers of uncertainties.

In general, BB emission inventories are based on bottom-up or top-down methods to infer the emission source intensity. The bottom-up approach, also known as the fire detection and/or burned area method, estimates emissions based on surface data such as fuel loading, active fire counts, and/or burned area. Currently, the widely used BB inventories based on the bottom-up approach include Duncan (Duncan, 2003), GFED (van der Werf et al., 2006, 2010a, 2010b, 2017), FINN (Wiedingmyer et al., 2011), Global Inventory for Chemistry-Climate Studies-GFED4S (G-G) (Mieville et al., 2010). The top-down approach uses satellite observations of fire radiative power (FPR), a method to measure the radiative energy release rate of burning vegetation, to estimate emissions by fuel consumption. The BB inventories based on the top-down method include Arellano (Arellano Jr et al., 2004; Arellano Jr and Hess, 2006), GFAS (Kaiser et al., 2012), Fire Energetics and Emission Research (FEER) (Ichoku and Ellison, 2014), QFED (Darmenov et al., 2015), the Fire Emissions Estimate Via Aerosol Optical Depth (FEEV-AOD) (Paton-Walsh et al., 2012) and the recently released VIIRS-based Fire Emission Inventory version 0 (VFEI0) (Ferrada et al., 2022). On a global scale, the average annual BB emissions of CO and OC can differ by a factor of 3 to 4, with the global emissions fluctuating in the range of 280-580 Tg yr^{-1} and 13-50 Tg yr^{-1} respectively. The bias may be even greater when focusing on emissions in specific regions (Bian et al., 2007; Liousse et al., 2010; Williams et al., 2012; Carter et al., 2020; Lin et al., 2020b; Liu et al., 2020b). For example, the estimated CO emission of Arellano inventory in South America during the burning peak season of September 2000 is four times greater than that of GFED1 inventory (Bian et al., 2007). A recent study even found that since 2008, OC emissions from QFED2.5 in the Middle East are approximately 50 times larger than those from GFED3 and GFED4 (Pan et al., 2020).

Several previous studies have analyzed the reason for the huge emission bias. According to Darmenov et al. (2015), the emissions E_i (mass of pollutant i) is the sum of the products of the emission factor (EF) and the dry matter (DM) for each biome. While earlier studies suggested that the uncertainty in BB emissions arises mainly from differences in emission factors (e.g., Alvarado et al., 2010; Akagi et al., 2011; Urbanski et al., 2011), more recent studies point out that uncertainty in dry matter also plays an important role (Paton-Walsh et al., 2010; 2012; Carter et al., 2020). For example, Paton-Walsh et al. (2012) assessed the difference in CO emissions from the February 2009 Australian fire and found that total CO emissions in GFED3.1 were roughly three times higher than that in FINN1, with DM contributing up to 80%. Carter et al. (2020) evaluated emissions from various North American BB inventories over the period 2004-2016 and found that changes in DM were very close to the emission trend, suggesting that uncertainty in potential DM across North America was the primary factor, rather than EF.

The accuracy of BB inventories is influenced by land cover and land use (LULC) data, impacting both EFs and DM (Wiedinmyer et al., 2006; Ferrada et al., 2022). In a study by Wiedinmyer et al. (2006), three distinct LULC products were employed to drive a regional BB emissions model. The variations in LULC products led to discrepancies in fuel consumption, resulting in an annual bias of up to 26% in North and Central America. Moreover, EFs are closely tied to different biomes, introducing uncertainty into BB emission inventories with varied biome classifications (Ferrada et al., 2022). In addition to LULC products, uncertainties are introduced by fire detection products (such as FRP and burned area products), affected by factors such as satellite transit time and cloud

obscuration. For example, Paton-Walsh et al. (2012) found that in an Australian fire called "Black Friday" in February 2009, the burned areas of FINN1 were barely half of that of GFED3.1. Liu et al. (2020b) reported that compared with the active fire area used in FINN1.5, the burned area product selected by GFED4s is less sensitive to the satellite overpass time and cloud obscuration. These results indicate that LULC and fire detection products are key factors leading to bias in BB emission estimation.

Although previous work has generated biomass burning emission inventories and attempted to reduce their uncertainties (Duncan, 2003; Arellano Jr et al., 2004; Arellano Jr and Hess, 2006; van der Werf et al., 2006, 2010a, 2010b, 2017; Bian et al., 2007; Mieville et al., 2010; Wiedingmyer et al., 2011; Kaiser et al., 2012; Paton-Walsh et al., 2012; Ichoku and Ellison, 2014; Darmenov et al., 2015; Liu et al., 2018; Ramnarine et al., 2019; Carter et al., 2020; Lin et al., 2020b; Liu et al., 2020b; Pan et al., 2020; Zhang et al., 2020; Ferrada et al., 2022), they did not analyze the reasons why DM and EF exhibited large differences among various emission inventories, which may vary over time and location. Here, this study aims to explore the underlying reasons for the differences in BB emission inventories in major combustion regions around the world, thereby attempting to reduce the uncertainties of the impact of BB emission inventories on model results. To minimize the interference of anthropogenic emissions on model results, we selected combustion regions satisfying the following conditions: (1) regional BB CO emissions above 20 Tg yr^{-1}; (2) BB CO emissions contribute more than 70% of the total. We ultimately selected seven major burning areas as shown in Fig. 1, including Boreal North America (BONA), Southern Hemispheric South America (SHSA), Northern Hemispheric Africa (NHAF), Southern Hemispheric Africa (SHAF), Boreal Asia (BOAS), Southeast Asia and India (SEAS), and Equatorial Asia (EQAS).

In this study, we compare several widely used datasets (FINN1.5, GFED4s, and QFED2.5) and the recently released VFEI0. The former two datasets are based on the bottom-up method, while the latter two are based on the top-down method. Specific details of these BB inventories are described in Section 2. In section 3, we explore the differences in CO and OC emissions among the four inventories, examining the contributions of DM and EFs to these differences, respectively. For the first time, we evaluate the biases of CO column concentrations and AOD driven by BB inventories in the CESM2-CAM6 model. Based on our findings, we provide recommendations on which inventory should be adopted across various regions. Section 4 presents the conclusion and discussion, and our research is expected to offer insights into reducing the uncertainties with BB emission datasets.

2 Data and Methodology

2.1 Biomass Burning emission inventories

We simultaneously diagnosed the differences between two bottom-up approach inventories and two top-down approach inventories, including FINN1.5, GFED4s, and QFED2.5, which are commonly used in the current atmospheric model, as well as the recently released VFEI0. Details about the emission inventories and the satellite products they use are listed in Table 1 and Text S1 in supplementary.

Bottom-up (Burned Area) inventories

In this study, both FINN1.5 and GFED4s adopt a bottom-up approach (also called the Burned Area method), and the details are shown in Table 1. FINN1.5 uses the MODIS (Moderate Resolution

Imaging Spectroradiometer) product MCD14DL for burned area calculations. This active fire detection product monitors real-time fire points larger than 0.05 km^2. However, it is important to note that if a fire occurs when the satellite is not in transit or is obscured by clouds during transit, it will not be detected (Firms, 2017). Additionally, FINN1.5 assumes that every fire detected at the equator (30°N-30°S) will persist the next day at half the size of the previous day (Table 1). However, this assumption may not accurately reflect real-world conditions (Wiedinmyer et al., 2011; Pan et al., 2020). The land cover classification in FINN1.5 is based on MCD12Q1 (IGBP, version 2005). According to the IGBP land cover classification, each fire is initially assigned to one of 16 land use/land cover (LULC) classes, and then lumped into six generic categories including tropical forest, temperate forest, boreal forest, savanna and grasslands, woody savannas and shrublands, and cropland (Fig. S1, Wiedingmyer et al., 2011). Emission factors (EFs) for various gaseous and particulate species are determined from a dataset compiled by Akagi et al. (2011) and Andreae and Merlet (2001), with these EFs varying for different LULC types. Currently, FINN1.5 provides daily global emissions from biomass burning since 2002, including 41 species, with a spatial resolution of 1 km^2 (Table 1).

GFED4s differs in that it primarily uses the MCD64A1 Collection 5.1 burned area product (Giglio et al., 2013; Randerson et al., 2018), capable of detecting fires larger than 500 m × 500 m. For small fire areas, GFED4s incorporate active fire detection products (MOD14A1 and MYD14A1), compensating to some extent for the lower spatial resolution of the original product MCD64A1 (van der Werf et al., 2017). In general, burned area products reduce uncertainty in fire detection due to satellite non-transit and cloud/smoke obscuration when a burn occurs by identifying day-to-day surface variations, such as charcoal and ash deposition, vegetation migration, and changes in vegetation structure (Boschetti et al., 2019). Similar to FINN1.5, each fire in GFED4s is initially assigned to one of 16 LULC subcategories and then lumped into six categories, with the inclusion of an additional biome, peatland (Fig. S1). EFs for various species follow Akagi et al. (2011) and Andreae and Merlet (2001), varying across different biome categories. Currently, GFED4s provide daily global emissions from biomass burning since 1997, including 27 species, with a spatial resolution of 0.25° × 0.25° (Table 1). However, since 2017, the DM provided by GFED4s is derived from a linear relationship between past emissions and MODIS FRP data for the period 2003-2016.

Top-down (Fire Radiative Power) inventories

In this study, both QFED2.5 and VFEI0 use a top-down approach known as the Fire Radiative Power (FRP) method. In contrast to the bottom-up approach, the top-down approach relies on satellite products detecting fire-radiated power rather than fire point detection. QFED2.5 uses MODIS Collection 6 MOD14/MYD14 level 2 products to estimate fire radiative power and pinpoint fire locations using MOD03/MYD03 (Darmenov and Silva 2015; Liu et al., 2020b). The FRPs are integrated over time to obtain fire radiative energy (FRE), which is converted to DM using an empirical coefficient α. The initial α values are obtained from Kaiser et al. (2009) and are adjusted monthly based on global emissions of GFED2 in 2003–2007. QFED2.5 classifies land cover using the International Geosphere-Biosphere Programme (IGBP-INPE) dataset, aggregating 17 land cover classes into four broad vegetation types (Fig. S1, Darmenov and da Silva 2015). Initially, EFs for various species in QFED2.5 also follow Akagi et al. (2011) and Andreae and Merlet (2001). But for certain species, including organic carbon (OC), black carbon (BC), ammonia (NH_3), sulfur

dioxide (SO_2), and particulate matter diameter < 2.5μm ($PM_{2.5}$), QFED2.5 incorporates a scaling factor to enhance the EFs. QFED2.5 provides daily global BB emissions since 2000, including 17 species, with a spatial resolution of 0.1° × 0.1° (Table 1).

VFEI0 also adopts the top-down method but uses VNP14IMG.001 FRP product from VIIRS I-band (Visible Infrared Imaging Radiometer). This product has a higher resolution (375 m at nadir) compared to MODIS (1 km resolution at nadir), enabling the detection of smaller and colder flames (Ferrada et al., 2022). VFEI0 uses an empirical coefficient α derived from the linear regression of GFED3.1 DM and VIIRS FRP to convert detected FRE into DM. VFEI0 uses MCD12C1 (IGBP, version 2015) as the underlying LULC data, supplemented by Köppen climate classification (Beck et al., 2018), defining ten subcategories in VFEI0 (Fig. S1). VFEI0 groups these subcategories into six biomes, corresponding to EFs provided by Andreae (2019). Currently, VFEI0 offers daily BB emission since 20 January 2012, covering 46 emitted species with a horizontal resolution of 0.005° × 0.005° (Table 1).

2.2 The calculation for EFs and DMs

To calculate regional EFs and DMs, we adopt the approach outlined by Carter (2020). Initially, we divide CO emissions per grid by the EF applied to each biome, yielding DM:

$$DM_{b,x} = CO_{b,x}/EF_b \quad (1)$$

where b represents one of the seven biomes in Fig. S1, and x represents the location grid. This calculation of DM using CO is reasonably representative, given that the inventories are not adjusted for CO emission factors. After calculating $DM_{b,x}$ for each grid, we derive a regional average emission factor by dividing total CO emissions by total DM for each major BB region:

$$EF_{CO} = \sum_{b,x} CO \,/\, \sum_{b,x} DM \quad (2)$$

These calculations enable us to discern the influence of LULC classification on BB emission inventories. For a specific biome type within a given region, we calculate EF by dividing the CO emissions of that particular biome classification by the sum of the value from each biome in the respective region:

$$EF_b = CO_b/\sum_b DM \quad (3)$$

where b represents one of the seven biome classifications in this study (Fig. S1).

Furthermore, for the two bottom-up inventories, we invert the fuel consumption for each vegetation biome b within a given area:

$$FC_b = DM_b/BA \quad (4)$$

Here, the DM corresponding to each biome in FINN1.5 and GFED4s is obtained using equation (1), and BA represents the total burned area derived from the emission inventory.

2.3 Quantitative statistical methods

As described in section 2.1, fire detection is greatly affected by cloud/smoke obscuration in the bottom-up approach. For example, if there are clouds/smoke at high altitudes while fire occurs on the ground, the MCD14DL active fire detection product used in FINN1.5 may miss these fire points. In addition, the combustion that is too small in size and too low in temperature, cannot be effectively monitored due to the low brightness temperature contrast with the surrounding environment. In contrast, the burned area product (mainly MCD64A1) used by GFED4s determines the burning information based on the changes such as surface albedo, and is, therefore less affected by

clouds/smoke. For inventories based on the top-down approach, the emission inventories also differ to a large extent due to the cloud/smoke obscuration, since QFED2.5 uses a "sequential method" to correct for missing FRPs during cloud/smoke obscuration, whereas VFEI0 does not. Thus, in this study, the symmetrical mean absolute percentage error (SMAPE) and Pearson's R are used to assess the difference in sensitivity to clouds/smoke between the two BB products based on the bottom-up (or top-down) approach. The specific algorithm is as follows:

$$\mathrm{SMAPE} = \frac{100\%}{n} \sum_{i=1}^{n} \frac{|X-Y|}{(|X|+|Y|)/2}, \quad (5)$$

$$R = \frac{\sum_{i=1}^{N} |(X-\bar{X})\cdot(Y-\bar{Y})|}{\sqrt{\sum_{i=1}^{N}(X-\bar{X})^2 \cdot \sum_{i=1}^{N}(Y-\bar{Y})^2}}, \quad (6)$$

where X and Y are fire detection data from two different datasets (e.g. burned area from FINN1.5 and GFED4s or FRP from VFEI0 and QFED2.5). We divided these fire detection data into three groups according to the cloud fractions less than 0.4, 0.4-0.7, and greater than 0.7, and the number n represents valid samples in different cloud fraction groups. SMAPE ranges from 0% to 200%, with smaller values indicating smaller differences, while Pearson's R ranges from 0 to 1, with smaller values implying less correlation.

In order to quantify the effect of cloud obscuration on BB datasets, we selected the most intensely burning regions in BONA in July for this study. For consistency, we re-interpolated the fire detection data used in the four BB datasets, as well as the MODIS MCD06 cloud fraction data, to the same horizontal resolution (0.25° × 0.25°). Considering the continuity of combustion, we took every 5° × 5° as a sample area in the northern U.S. to ensure that if a large burn occurred, the area would be detected to some extent, avoiding errors due to differences between the inventories. At the same time, we excluded the samples at the same time and location, where the emissions are all zero. Finally, a total of 1888 samples were obtained for the burned area group, with 534, 541, and 813 samples for low (<0.4), medium (0.4-0.7), and high (>0.7) cloud fraction, respectively. A total of 1,682 samples were obtained for the FRP group, with 860, 390, and 432 samples under low, medium, and high cloud fraction, respectively. It is worth noting that we use the average FRP of MOD and MYD for QFED2.5 since the VFEI0 FRP is the average between day and nighttime observations. Moreover, our approach cannot rule out the case of missing measurements when two sets of BB inventories are both obscured by the cloud. However, the main goal of this paper is to explore the causes of uncertainties in emission inventories, the specific case of omission due to cloud obscuration depends on the development of satellite detection technology and is not part of the purpose of this study.

2.4 CESM2-CAM6 model

The Community Earth System Model version 2.1 (CESM2) is a new generation of the coupled climate/Earth system models developed by National Center for Atmospheric Research (NCAR). In this study, we used the global Community Atmosphere Model version 6 (CAM6) (Danabasoglu et al., 2020). Gas-phase chemistry was represented by the Model for Ozone and Related chemical Tracers tropospheric chemistry (MOZART-T1, Emmons et al., 2020). The wet deposition of soluble gaseous compounds in CAM6-Chem is based on the scheme of Neu and Prather (2012), which describes the process of in-cloud cleaning and under-cloud cleaning. The formation of secondary organic aerosols (SOA) is from a volatility basis set (VBS) approach developed by Tilmes (2019).

Properties and processes of aerosol species of black carbon (BC), primary organic aerosols (POA), SOA, sulfate, dust, and sea salt are calculated by Modal Aerosol Module (MAM4) described by Liu (2016). CAM6 uses a horizontal resolution of nominal 1° (1.25° × 0.9°, longitude by latitude) and 32 vertical levels from the surface to 2.26 hPa (~40 km).

In this study, four BB emission inventories (FINN1.5, GFED4s, QFED2.5, and VFEI0) are re-gridded to a horizontal resolution of 1.25° (longitude) × 0.9° (latitude), and then applied to the model. All simulations were performed for five years, while horizontal winds and temperature were nudged toward the Modern-Era Retrospective analysis for Research and Applications, version 2 (MERRA-2) reanalysis data (GMAO, 2015) for every 6 h. Simulations are conducted for 2012-2016, with the first year used for initialization and model spin-up. Daily BB emissions were applied in this study, whereas the vertical distribution of fire emissions was followed Freitas et al. (2006, 2010). Anthropogenic and biogenic emissions in this study are from the Community Emissions Data System (CEDS) and Model of Emissions of Gases and Aerosols from Nature version 2.1 (MEGANv2.1), respectively, at 2010 levels (Guenther et al.,2012; Hoesly et al., 2018).

2.5 Measurement data

The Tropospheric Pollution Measurement Instrument (MOPITT) is aboard the Earth Observing System (EOS)/Terra satellite launched by NASA (Warner, et al., 2001). MOPITT is the first instrument to observe the global concentration and currently provides column concentration and volume mixing ratio of global carbon monoxide (CO) since 1999. We used MOPITT CO gridded monthly means (Near and Thermal Infrared Radiances) V009 (MOP03JM_9; NASA Langley Atmospheric Science Data Center DAAC, retrieved from https://doi.org/10.5067/TERRA/MOPITT/MOP03JM.009), which has a horizontal resolution of 1° × 1°. It should be noted that to compare the CO column concentration simulated by CESM2-CAM6 with MOPITT CO, we calculated the simulated CO column concentrations by cumulative integration from 900 hPa to 100 hPa isobaric height (Deeter et al., 2022). We also used the daily AOD (550 nm) and cloud fraction data from MODIS products MOD08_D3 (MODIS/Terra Aerosol Cloud Water Vapor Ozone Daily L3; Platnick et al. 2015) and MCD06COSP (MODIS (Aqua/Terra) Cloud Properties Level 3 daily, Webb et al., 2017), respectively.

The observations of AERONET (http://AERONET.gsfc.nasa.gov/; Holben et al., 1998) from 12 sites are used in this study. These AERONET stations were selected since they are close to BB source regions. As marked in Figure 1b, these sites include sites in BONA (Yellowknife_Aurora (62.5°N, 114.4°W), Pickle Lake (51.4°N, 90.2°W)), BOAS (Tiksi (71.6°N, 128.9°E), Yakutsk (61.7°N, 129.4°E)), SHAF (Namibe (15.2°S, 12.2°E), Mongu Inn (15.3°S, 23.1°E)), SHSA (Alta Floresta (9.9°S, 56.1°W), Rio Branco (9.9°S, 67.9°W)), EQAS (Palangkaraya (2.2°S, 113.9°E), Jambi (1.6°S, 103.6°E)), SEAS (Omkoi (17.8°N, 98.4°E), Ubon Ratchathani (15.2°N, 104.9°E)).

All observed AOD represent real atmospheric conditions and therefore, in addition to BB aerosols, biogenic aerosols, anthropogenic aerosols, dust, and sea salts are also integrated in MODIS and AERONET datasets.

3 Comparative analysis of emission inventories

CO and OC are the main species emitted from biomass burning (Westerling et al., 2010; van der Werf et al., 2010b; Carter et al., 2020) but emissions vary widely. In this study, we compare the

differences in CO and OC emissions (representing gaseous and particulate pollutants, respectively) in four BB inventories, and investigate in detail the key reasons for the differences in emission inventories.

3.1 The contribution of dry matter and emission factors to the difference in CO emission

The total global CO emissions from the four BB emission inventories selected for this study are in the range of 252-336 Tg, with GFED4s being the highest and FINN1.5 the lowest. To quantify the differences in CO emissions among four datasets, we use the standard deviation (SD) to characterize the absolute difference, and the coefficient of variation (cv, calculated as the ratio of SD to the mean) to characterize the relative differences (Fig. 2a). The larger the cv, the greater the difference between emission inventories. We have ranked the major seven BB regions in the world according to the differences in CO emissions between the four sets of inventories, with the differences being, in descending order, EQAS, BONA, SEAS, SHAF, NHAF, BOAS, and SHSA.

This study points to a high variability of different BB emission inventories in EQAS, which is inconsistent with previous studies (Liu et al., 2020b; Pan et al., 2020). Previous studies mainly focused on emission differences of particulate pollutants, such as BC and OC (Bian et al., 2007; Paton-Walsh et al., 2012; Carter et al., 2020; Lin et al., 2020b; Pan et al., 2020), thus assuming that the inventory differences in Equatorial Asia are smaller than those in Southern Hemispheric Africa and Northern Hemispheric Africa. In contrast, this study analyzes the differences between particulate and gaseous pollutant emissions separately when comparing the differences in BB emission inventories. For example, GFED4s classify a large portion of EQAS land cover as peatland (Kasischke and Bruhwiler, 2002; Stockwell et al., 2016; van der Werf et al., 2006, 2010a, 2010b, 2017) and suggest that this organic matter-rich soil emits a large amount of CO when burned. The other three inventories either do not include peatland (FINN1.5 and QFED2.5) or only consider peatlands as a small fraction of the burned area in EQAS (VFEI0), thus estimating CO emissions much smaller than GFED4s. In addition, the extent of peatland fires in EQAS increased significantly during the strong El Niño event (Page et al., 2002). Considering that a strong El Niño event also occurred in 2015-2016, these increases in peatland fires further amplify the discrepancy between GFED4s and other emission inventories on CO estimates.

As shown in Fig. 2, the distribution pattern of DM differences is very similar to that of CO emission differences, indicating that DM is the main reason for dominating the difference in the four emission inventories. In comparison, the difference in DM contributes 50-80% to the regional CO emission differences, and the comprehensive EFs contributes the remaining 20-50%. However, in EQAS, BONA, and BOAS, the contribution of comprehensive EFs to BB emission differences in four datasets is comparable to that of DM (Fig. 2). In the following sections, we will further analyze the main causes of the differences for DM and EFs.

3.2 Primary causes of DM inconsistency in the bottom-up inventories

To investigate the underlying causes of the differences in DM, we first compared DM between emission inventories produced by the bottom-up and up-down approaches. The difference in DM estimated by the top-down method is small, and the DM ratio of QFED2.5 to VFEI0 does not exceed two times in different regions. However, DM estimated by the bottom-up approach varied widely, with DM ratio as high as 4.7 in BONA for GFED4s and FINN1.5 during the 2013-2016 fire season.

Therefore, we need to focus on the main reasons for DM variance in emission inventories based on bottom-up approach.

According to Eq. (2), DM equals the product of the burned area, fuel load, and FB in the bottom-up inventories, with the product of the last two terms being fuel consumption. Fig. 3 compares the burned area and fuel consumption of GFED4s and FINN1.5 emission inventories for the seven largest BB regions. The ratio GFED4s/FINN1.5 represents the relative difference in burned area or fuel consumption between the two emission inventories. In general, the difference in burned area between the two inventories varies greatly with latitude, and the ratio of GFED4s to FINN1.5 fluctuates in the range of 0.28-1.94. In contrast, differences in fuel consumption between the two inventories were more consistent, with GFED4s consistently having higher fuel consumption than FINN1.5 in all regions except SEAS. In the next sections, we discuss the main reasons for the differences in burned area and fuel consumption between the two datasets.

3.2.1 Effect of land cover on burned area

As shown in Fig. 3a, the differences in the burned area between the bottom-up emission inventories are highly variable. At high latitudes, the burned area of GFED4s is significantly higher than that of FINN1.5, especially in BONA, where the burned area of GFED4s is twice that of FINN1.5. In contrast, the burned area of GFED4s in the equatorial region is much lower than that of FINN1.5, and even 60% smaller in EQAS. This is a result of the difference in fire detection between the two datasets. As shown in Table 1, FINN1.5 uses the MCD14 DL fire point product, while GFED4s uses the hybrid burned area product, mainly using MCD64A1 combined with fire point products MOD14A1/MYD14A1 to enhance the detection of small fires.

These two sets of products have their advantages in detection ability under different vegetation type conditions. The hybrid burned area product detects burned areas over a period of time (up to days), while the fire point product detects burned areas primarily in near real-time (Roy et al., 2008). In addition, the burned area used in GFED4s (hybrid burned area product) is not affected by the vegetation canopy when the leaf area index (LAI) is less than 5. Therefore, a higher burned area is estimated in GFED4s in BONA and BOAS than in FINN1.5. However, in areas with more broadleaf forests and grasslands such as EQAS, SEAS, and SHSA (Fig. S2), the MCD14DL fire point product used in FINN1.5 performed better in capturing understory fires that occurred in closed canopies (Cochrane and Laurance, 2002; Cochrane, 2003; Alencar et al., 2005; Roy et al., 2008). It also has an advantage in capturing sporadic and fragmented small fires in grasslands and agricultural fields due to its high resolution (Liu et al., 2020b). Furthermore, FINN1.5 assumes that each detected fire in the equatorial region will continue to burn for 2 days, and that the next day's fire will continue to be half the size of the previous day (Table 1). Thus, the burned area of FINN1.5 in the tropical zone is 2.6 times higher than that of GFED4s, which is consistent with previous studies (Wiedinmyer et al., 2011; Pan et al., 2020). At the equator, the burned area in grassland/agricultural fields and forests estimated by FINN1.5 is 1-3 and 4-6 times higher than in GFED4s, respectively (not shown).

It is worth noting that in Africa (NHAF and SHAF), although the dominant burnable vegetation is grassland (Fig. S2), unlike the sporadic small fires that occur in grassland in the other five regions, large continuous fires often occur in African Savannas (Liu et al., 2020b). Therefore, the hybrid burned area product used in GFED4s is more effective in detecting all fire events occurring over time, with 10-20% higher burned area than FINN1.5.

3.2.2 Effect of cloud obscuration on burned area

In addition to the vegetation, cloud occlusion can likewise bias the satellite detection of burned area. Figure S3 shows the time series of AOD measured by satellite or ground-based data at the Pickle Lack site of BONA from June to August 2013. In contrast to the high AOD values observed for the AERONET network, MODIS AOD often in missing measurements when the MODIS cloud fraction is larger than 0.5. Furthermore, AERONET AOD varies dramatically over a short period, suggesting that different detection principles (such as detecting fire points in near real-time during satellite overpass time, or estimating the accumulation of burned area over time through changes in surface albedo over multiple satellite overpass times) can significantly affect the burned area product under high cloud fraction/smoke conditions (Paton-Walsh et al., 2012; Liu et al., 2020b; Pan et al., 2020). Although some assumptions are made in FINN1.5 in the equatorial regions as described above to improve the effect of cloud obscuration on burned area detection, these assumptions are not used for mid- and high-latitudes. GFED4s uses a hybrid burned area product and is relatively unaffected by cloud obscuration. By fusing the MCD64A1 with MOD14A1/MYD14A1 products with multi-temporal satellite data, GFED4s is able to determine the approximate date and extent of fires through post-fire ash deposition, vegetation migration, and land surface changes (van der Werf et al., 2017; Boschetti et al., 2015, 2019).

To quantitatively assess the impact of cloud obscuration on different emission inventory estimates, we perform analyses in areas with high cloud fraction (Fig. S4), intense biomass burning, and unaffected by the smoothing hypothesis used in FINN1.5. We selected the regions of North America with the most intense biomass burning (Alberta and Saskatchewan, Canada, 50°-70°E, 100°-130°W, Fig. S5), and analyzed the relationship between the burned area and cloud fraction for bottom-up inventories during July from 2013 to 2016 (Fig. S6). As shown in Fig. 4, with the increase in cloud fraction, the SMAPE of the two bottom-up emission inventories increases from 150% to 180%, while the Pearson correlation declines from 0.85 to around 0.75. These results demonstrate that the uncertainty in the burned area for two bottom-up emission inventories increases by ~20% during high cloud fraction compared to low cloud fraction conditions.

3.2.3 Causes of Fuel Consumption differences

Fuel consumption is another factor that affects DM differences between two BB emission inventories. As shown in Fig. 3b, the fuel consumption of GFED4s is 30-75% higher than that of FINN1.5 in almost all BB areas except SEAS. The difference in fuel consumption between the two emission inventories is larger in the tropics than in the high latitudes. As shown in Fig. 5, at high latitudes (e.g., BONA and BOAS), and in the equatorial region (such as EQAS), relatively high fuel consumption comes from peatlands in GFED4s. According to previous studies, peatlands, a type of soil rich in organic matter, store large amounts of carbon underground (van der Werf et al., 2010b, 2017; Gibson et al., 2018; Kiely et al., 2021; Vetrita et al., 2021), and emit large amounts of CO when burned. Peatlands contribute 30-60% of the total fuel consumption in BONA, BOAS, and EQAS (Fig. 5a-c).

Besides peatlands, GFED4s tends to have higher fuel consumption than FINN1.5 due to forest contributions. Forests (including tropical, temperate, and boreal forests) account for more than 50% of the fuel consumption in all burning regions except EQAS, where peatlands dominate the fuel consumption. Moreover, forest fuel consumption in GFED4s is generally much higher than in

FINN1.5 except in BOAS and SEAS (Fig. 5). Since fuel consumption is equal to the product of fuel load and FB (the percentage of specific plants that can be adequately burned, Eq. 2), different vegetation classifications may be responsible for large differences in fuel consumption between emission inventories. For example, for woody vegetation such as forests, GFED4s assumes a range of FB between 40-60% for temperate and tropical forests and 20-40% for boreal forests, while FINN1.5 assumes that all woody vegetation burns no more than 30% (van der Werf et al., 2010; Wiedinmyer et al., 2011). Thus, in terms of FB alone, the forest fuel consumption of GFED4s is therefore 0.67-1.3 times greater than that of FINN1.5, which is one of the main reasons for the difference in fuel consumption.

3.3 Primary causes of DM inconsistency in the top-down approach

We also analyze the causes of the difference in DM between BB emission inventories estimated by the top-down method. According to Eq. (3), it is evident that the empirical factor and the radiative energy of the fire are the key factors that cause the discrepancy in the top-down emission inventories. The QFED2.5 and VFEI0 inventories we have chosen use different satellites for the fire detection products. For example, for the fire radiative power product, QFED2.5 is based on the Moderate Resolution Imaging Spectroradiometer (MODIS) inversion of the NASA Terra and Aqua combined satellites, while VFEI0 is based on the Visible Infrared Imaging Radiometer (VIIRS) inversion of the combined polar-orbiting satellites Suomi NPP and NOAA-20, although the algorithms are similar. However, there are systematic deviations due to different satellites, specific tests and metadata, and resolutions. The VIIRS 375 m fire product used by VFEI0 has a finer resolution and is more advantageous for small fire spot detection than other coarser resolution (1 km) fire spot detection products. The FRP density used in VFEI0 is much higher than that of QFED2.5 due to the fine horizontal resolution.

The estimations of FRP and DM are strongly influenced by the horizontal resolution of satellite products. For example, in the BONA region during July (the month with the most intense burning at the position of 50°-70°N, 100°-130°W), the total QFED FRP (average FRP measured by MOD and MYD) is 1.5 times higher than VFEI0 (Fig. S7). Additionally, the differing α values between QFED2.5 and VFEI0 in BONA can potentially result in higher DM in QFED2.5 compared to VFEI0 by a factor of 1.3-3.8. However, the actual DM in the QFED2.5 inventory is 30% lower than in VFEI0. The relatively high FRP density used in VFEI0 (Fig. S8) results in a higher DM than in QFED2.5 due to its superior horizontal resolution, enabling the precise delineation of fire areas. It is important to note that while the empirical factor also influences the amount of DM, its impact should not be as significant as the difference caused by the horizontal resolution of satellite products (Kaiser et al., 2012; Darmenov et al., 2015; Ferrada et al. 2022).

Previous studies have shown that cloud occlusion also causes bias in FRP detection (Liu et al., 2020b). We also take BONA as a pilot region to analyze the influence of cloud fraction on FRP in QFED2.5 and VFEI0. According to Fig. 5c-d, the SMAPE of the two emission inventories rises as the cloud fraction increases, and the Pearson correlation is noticeably low under the maximum cloud fraction. While QFED2.5 uses the "sequential approach" (section 2.1) to correct for the missing FRP in cloud-obscured fires, this correction is not considered in VFEI0. Therefore, although the two top-down emission inventories use similar algorithms, significant bias occurs under high cloud fraction conditions, with QFED2.5 estimating DM much higher than VFEI0.

3.4 Primary causes of EF inconsistencies

Although DM differences dominate the inconsistencies of CO emissions across major BB regions, the contribution of EFs is still not negligible in some regions. For example, in EQAS, BONA, and BOAS, the contribution of EFs is up to 50%, which is comparable to that of DM. The comprehensive EFs of GFED4s are higher in BONA, BOAS, and EQAS regions than in other inventories, with vegetation classification being one of the most important factors (Fig. 6). For example, in EQAS at low latitudes, peatlands in GFED4s account for 65% of the regional comprehensive EF. In contrast to GFED4s, FINN1.5, and QFED2.5 do not consider this organic matter-rich land as a source of burning, and they classify this category of land cover type as savanna or grass. The CO emission factor for peatlands is four times higher than the CO emission factor for savanna or grass (Table 2), ultimately making the comprehensive EF for GFED4s 60-70% higher than that of the other three datasets. It is worth noting that although the classification of Peatland exists in VFEI0 (Ferrada et al., 2022), due to differences in terrestrial ecological divisions (Olson et al., 2001; http://www.worldwildlife.org/science/data/item1875.html), peatlands identification areas are much smaller than GFED4s inventory. Therefore CO emissions from peatlands in GFED4s are much higher than in the VFEI0 inventory (Figure 3-9a; Ferrada et al., 2022).

In both BONA and BOAS, we find that the comprehensive EFs in the four datasets are ranked as follows: GFED4s>FINN1.5>QFED2.5>VFEI0, where the EF of GFED4s is about 1.5 times higher than that of VFEI0. Unlike the low-latitude regions, the classification of forests in different emission inventories is the main reason for the difference in comprehensive EF in high-latitude regions. At high latitudes (50° - 70°N), GFED4s, QFED2.5, and FINN1.5 identify more forests than VFEI0 (Fig. S1) because the former three classify some shrubs (e.g., closed shrublands and woody savanna) as forests, while the latter classify them as grassland. Forests contribute to 70% or more of the comprehensive EFs at high latitudes in the first three emission inventories, but only 8% to the comprehensive EF in VFEI0. The remaining gap in the absolute contribution of forests is caused by the difference in the selected emission factors and the horizontal resolution of the satellite products.

3.5 Contribution of DM and EFs to differences in OC emissions

The above analysis completes the comparison of gaseous pollutant CO among different emission inventories. In this section, we will take OC as an example to compare the emission differences of particulate pollutants. As shown in Fig. 7, the global OC emissions of four datasets range from 14.9 to 42.9Tg, with the highest emissions from QFED2.5, which is consistent with previous studies (Carter et al., 2020; Pan et al., 2020). According to the statistical method in section 3.1, we quantified the magnitude of OC emission differences between regions and ranked them as follows: BONA>BOAS>NHAF>SHAF>SEAS>SHSA>EQAS. Compared to the CO emission differences (Fig. 2), the difference in OC emissions becomes larger for BOAS and smaller for low latitude regions of SEAS and EQAS. Since DM should be consistent in the same emission inventories for a given time and area, the magnitude of emissions for different species depends on changes in emission factors. Considering that the emission factors of aerosol-related emission species such as OC, BC, NH_3, SO_2, and $PM_{2.5}$ have been corrected based on the satellite retrieved AOD of the QFED2.5 emission inventory (Table 2), the EFs of OC in QFED2.5 are much higher than that of the other three emission inventories (Fig. 7b). As a result, the OC EFs in the QFED2.5 emission inventory were enlarged by a factor of 1.8-4.5 times through the correction of BOAS, SEAS and

EQAS (Table 2). In contrast, the other three emission inventories were not corrected for OC EFs.

Unlike the CO EFs, the OC EFs of GFED4s in equatorial regions are largely consistent with the FINN1.5 and VFEI0 emission inventories. Although burning organic matter-rich soil substrates is generally thought to release large amounts of CO, their ability to release OC is similar to that of vegetation such as shrubs and some forests. Thus, despite CO emissions bias in EQAS being largely affected by peatlands, differences in OC emissions among the four inventories are not significant.

Compared with Pan et al. (2020), it is obvious that the top-down approach will not lead to an increase in emission deviation of the particulate-phase species. The correction of EFs, however, is the root cause of the increased bias in OC emissions. Pan et al. (2020) reported that QFED2.5 and FEER1.0 had the highest global OC emissions, while GFAS1.2 had much lower OC emissions. In this study, the largest OC emission also appears in QFED2.5, but the global total OC emissions of the recently released VFEI0 are relatively low.

4 Model evaluation based on emission inventories application

4.1 Comparison of simulations with MOPITT CO

One of the main goals of this study is to provide a confidence assessment of the BB emission inventories by comparing model simulations with observations. A comparison between model simulations using different emission inventories and ground-based/satellite-retrieved data for the respective fire seasons (Table 3) of the main BB regions is explored below. In this study, we compared the model results with measurements from two perspectives: the spatial distribution of BB pollutants, and the time-varying characteristics of BB pollutants.

Figure 8 depicts the spatial distribution of CO column burdens in SHSA and SHAF during the fire seasons. In SHSA, the simulated CO column burdens using different emission inventories are all consistent with the spatial distribution pattern of MOPITT CO column burden, with the peak value located in the Amazon rainforest. However, the central value of MOPITT CO column burden is as high as 2.8×10^{18} molecules cm^{-2}, which is slightly higher than the simulated results. Among the four sets of emission inventories, the peak amplitude and spatial distribution of simulated CO column burdens are closest to the satellite-retrieved data after applying the GFED4s and VFEI0. In SHAF, however, the model underestimated the peak CO column burden after applying all emission inventories except VFEI0.

In addition to SHSA and SHAF, a comparison of regionally averaged CO column burdens between our simulations and MOPITT CO in major BB regions is also shown in Table 3. In the Northern Hemisphere, our simulations are significantly underestimated compared to MOPITT CO, while those in the Southern Hemisphere are consistent with satellite retrievals. Surprisingly, the simulated spatial distributions and magnitudes of CO in the Southern Hemisphere using the recently released VFEI0 agree very well with observations. In contrast, the underestimation of CO concentrations in the Northern Hemisphere is partly due to uncertainty in anthropogenic emissions, as we assume anthropogenic emissions at 2010 levels, which are lower than those during the 2013-2016 period.

Note that simulated CO concentrations are 30-40% lower than MOPITT CO at high latitudes. Besides the impact of emission inventories, there are also large uncertainties in satellite-retrieved CO concentrations (Lin et al., 2020a; Pan et al., 2020). In addition, OH loss, long-range transport, and photochemical reactions involved in the CESM2-CAM6 model simulations also lead to

uncertainties in simulated CO. For example, MOZART-4x contains an additional OH oxidation pathway for CO, which may lead to lower CO concentrations (Lamarque et al., 2012; He and Zhang, 2014; Barré et al., 2015; Brown-Steiner et al., 2018; Emmons et al., 2020). In comparison, the simulated CO by using GFED4s is closest to the MOPITT CO value in terms of spatial distribution and peak magnitude at high latitudes in the Northern Hemisphere, which is superior to other emission inventories.

4.2 Comparison of simulations with MODIS AOD

We compared MODIS-derived aerosol optical depth (AOD) data with simulated AOD in major BB areas. Figure 9 shows the spatial distribution of AOD in SHSA and SHAF during their fire seasons. The simulated AOD is significantly higher than the MODIS AOD in SHSA. Note that primary organic aerosols (POA) associated with BB account for only 15-23% of the total AOD in Amazon, while secondary organic aerosols (SOA) account for approximately 50% of the total AOD. Furthermore, overestimation of simulated AOD occurs throughout the year, not just during the fire season. Considering the high biogenic emissions in this region, the overestimation of AOD could be attributed to the formation of biogenic SOA (He et al., 2015; Tilmes et al., 2019). In SHAF, the spatial distribution and magnitude of simulated AOD using GFED4s and VFEI0 are close to those of the MODIS AOD. In comparison, our results show that AOD is significantly underestimated using FINN1.5, but largely overestimated using QFED2.5.

Table 4 shows the mean values of model-simulated AOD and satellite measurements for each region during its fire season. The influence of the BB emission inventory has little effect on the simulated AOD value in the Southern Hemisphere, and the regional average AOD deviation is within 20%. In contrast, the average deviation of simulated AOD driven by four BB inventories can be as high as 40% in the high latitudes of the Northern Hemisphere. Comparatively, GFED4s and QFED2.5 are more suited for high latitudes in the northern hemisphere, whereas the VFEI0 is most suitable for the southern hemisphere for AOD simulations. In Africa, QFED2.5 is not recommended due to its considerable overestimation.

4.3 Comparison of simulations with ground-based measurements

In the above sections, we merely discussed the spatial distribution and the magnitude of pollutants during fire seasons. To further analyze whether each dataset can effectively capture the instantaneous combustion of BB, we compared the value of simulated daily AOD with that of ground-based observation (Fig. 10). To be more representative, we selected stations in each BB region with a large amount of data during fire season, allowing a comprehensive assessment of the global BB emission inventories. The specific locations of the selected 12 AERONET sites are shown as red triangles in Fig. 1b.

At EQAS sites such as Palangkaraya and Jambi, the observed AOD from September to November 2014/2015 is generally higher than 1, with peaks exceeding 5, reflecting the intense BB events (Fig. 10a-b). Only simulations using GFED4s are consistent with observed AOD during strong BB events, with a slight underestimation of 33-38%, while none of the other simulations could capture the BB process. Considering the significant contribution of peatlands to BB emissions in EQAS in GFED4s, our results suggest that it is important to include the burning of organic matter-rich soils in BB emission inventories. At SEAS sites such as Omkoi and Ubon Ratchathani, the peak AOD occurs

from February to April at a value of about 2, and all simulations applying the four emission inventories capture the observed changes in AOD (Fig 10c-d). However, due to the uncertainty of anthropogenic emissions, the simulated AOD is usually smaller than the actual observed value in EQAS. Note that simulations using QFED2.5 are most consistent with observed AOD during intense biomass burning events.

At the Namibe station of SHAF (Fig. 10e), the simulated AOD agrees best with the measured results after using FINN1.5 and GFED2.5, with NMB values within ±8%, indicating these two emission inventories can characterize the day-to-day variability of the intense BB process. However, Namibe is located downwind of the dust source, and dust aerosols contribute more than 50% to the total AOD in this area. To better evaluate the performance of the four BB emission inventories in SHAF, we chose another site, Mongu Inn, located in the interior of Southern Hemispheric Africa, where dust and sea salt accounted for 20-30% of the total AOD. At Mongu Inn, all simulations underestimate AOD by 46-71%, and only QFED2.5 and VFEI0 emission inventories can capture a few peaks during intense biomass burning events (Fig. 10f). In SHSA, while Figures 9 and 10h show an overall overestimation of simulated AOD compared to MODIS AOD, at the Brazilian Alta Floresta site east of the Amazon, simulated AOD agrees very well with the ground-based observations (Fig. 10g). In general, the simulations using the VFEI0 emission inventory for the Southern Hemisphere are close to the measurements.

At high latitudes, simulations driven by GFED4s and QFED2.5 better capture the observed peak AOD, with regional NMB values of less than 40% (Fig. 10i-l), suggesting that these two simulations can reproduce the intense BB process. In contrast, FINN1.5 and VFEI0 are obviously not suitable for describing the BB process in these sites, and the simulated AOD is underestimated by 60-80%.

5 Conclusion and Discussion

In this study, we examine four commonly used BB emission inventories (two bottom-up inventories (GFED4s and FINN1.5) and two top-down inventories (QFED2.5 and VFEI0)) to better understand the uncertainties associated with BB emissions. We analyze variations in CO and OC emissions across seven major BB regions worldwide from 2013 to 2016. We explore the differences between gaseous and particulate emission inventories, quantifying the impact of vegetation classification, cloud cover, and emission factors on inventory bias. Additionally, we apply these inventories to the global model CESM2-CAM6 to assess the model performance in simulating pollutants against satellite and ground-based observations.

The total global CO emissions exhibit significant variability among the four inventories, with annual averages ranging from 252 to 336 Tg, and a maximum deviation rate exceeding 30%. In certain regions such as BONA, changes in CO emissions are even larger, GFED4s emits 5.8 times more CO than FINN1.5. DM is identified as the primary contributor to variance among BB emission inventories, accounting for 50-80% of regional bias, while comprehensive EFs contribute the remaining 20-50%. Interestingly, the contributions of DM and comprehensive EFs to emission inventory differences are comparable across equatorial regions and Northern Hemisphere high latitudes.

The uncertainty in DM arises from underlying fuel consumption and burned area, linked to vegetation classification, fire detection product algorithm, and cloud/smoke masking. Vegetation classification significantly impacts fuel loading and the Fraction of Biomass burned, with discrepancies contributing to biases in fuel consumption. In regions at both low and high latitudes

(except Southeast Asia), FINN1.5 exhibits a fuel consumption term that is less than 50% of GFED4s, with the vegetation classification methodology contributing primarily to this bias. Different fire detection products introduce bias in estimated burned area, affecting uncertainty in DM. Satellite transit/cloud obscuration influences DM by affecting burned area/fire radiative energy. Cloud cover at high latitudes substantially impacts emission uncertainty, with bias increasing by 20% in July in BONA under higher cloud fraction.

We extend our analysis to particulate pollutants, using OC emissions as an example. Global average annual OC emissions vary widely among the four inventories, ranging from 14.9 to 42.9 Tg, demonstrating greater variability than gaseous species like CO. BB OC emissions exhibit large variability at high latitudes in the Northern Hemisphere, with QFED2.5 adjusting emission factors based on satellite aerosol optical thickness (AOD) to enhance particulate matter emissions.

Applying four BB emission inventories to CESM2-CAM6, we compare model-simulated CO column concentrations with the MOPITT satellite inversion CO column concentrations. According to our simulations, CO simulated using GFED4s is closest to satellite observations in almost all regions except southern Asia and Africa. We also compared model results with AOD retrieved from MODIS satellites or measured by AERONET. Simulated AOD at high northern latitudes is often underestimated when using current mainstream BB emission inventories. For example, the simulated regional average AOD is 8-46% lower than MODIS in North America. Unlike the high latitudes, the simulated AOD is significantly overestimated at the equator, and the regional average AOD simulated by the model in Northern Hemispheric Africa is 66-91% higher than MODIS. In addition, comparing model simulated AOD with AERONET ground-based observations, we find that GFED4s performs best in EQAS for daily variability during intense burning. In SEAS, although FINN1.5 can better represent the magnitude of the overall OC emissions in the BB season, QFED2.5 can capture the day-to-day variation characteristics of intense combustion. In the Southern Hemisphere, the latest VFEI0 emission inventory performs well, and the simulated AOD is able to capture the BB processes.

Our study assesses the global applicability of BB emission inventories and has some implications for future studies. Overall, GFED4s and QFED2.5 inventories for the northern high latitudes capture the magnitude and daily variation of OC emitted throughout the BB season. These two emission inventories outperformed the others when applied to studies of interactions between BB aerosol and weather/climate. In the Southern Hemisphere, the spatial distribution and daily variation characteristics of CO and AOD simulated by the model are closest to the observed values when the latest VFEI0 emission inventory is applied. For the equator, the situation is more complicated, and we recommend combining emission inventories according to the research objectives. For example, GFED4s performs best in day-to-day changes during intense burning in equatorial Asia. In Southeast Asia, combining OC magnitude in FINN1.5 and daily variation in QFED2.5 is the optimal choice.

It is worth noting that emission factors (as listed in Table 2) significantly contribute to the differences in BB emissions. However, actual emission factors vary widely depending on the different states of combustion (Pokhrel et al., 2021). Further study is needed to understand the impact of combustion efficiency on the BB EFs and optimize them.

Data availability. The biomass burning emission datasets used in this work are available from http://www.globalfifiredata.org (GFED4s), https://www.acom.ucar.edu/Data/fire/ (FINN1.5),

https://portal.nccs.nasa.gov/datashare/iesa/aerosol/emissions/QFED/v2.5r1/ (QFED2.5), and http://bio.cgrer.uiowa.edu/VFEI/DOWNLOAD/ (VFEI0). AOD and cloud fraction from MODIS dataset can be obtained from https://ladsweb.modaps.eosdis.nasa.gov/search/. MOPITT CO can be obtained from https://doi.org/10.5067/TERRA/MOPITT/MOP03JM.009. AERONET AOD is avaiable from https://aeronet.gsfc.nasa.gov/new_web/download_all_v3_aod.html. The Modern-Era Retrospective analysis for Research and Applications, version 2 (MERRA-2) reanalysis data is available from https://gmao.gsfc.nasa.gov/reanalysis/MERRA-2/. All data analyzed during the current study are included in this published article and its supplementary information. Raw model simulations are available from the corresponding author on reasonable request.

Author contributions. S. L. and A. D. designed the research, W. H. and S. L. conducted the data analysis and model simulations, W. H. and S. L. took the lead in writing the manuscript, with contributions from all authors.

Competing interests. The authors declare that they have no conflict of interest.

Acknowledgements. This work was supported by National Natural Science Foundation of China (grant number: 42325506, 42075095) and the International Cooperation project of Jiangsu Provincial Science and Technology Agency (BZ2017066).The numerical modelling was conducted on computing facilities at the High Performance Computing Centering (HPCC) at Nanjing University. The authors are grateful to the the AERONET networks for making their data available, part of the NASA Earth Observing SystemData and Information System (EOSDIS). We also thank the providers of biomass burning emission datasets of GFED, FINN, QFED and VFEI.

References

Adams, C., McLinden, C. A., Shephard, M. W., Dickson, N., Dammers, E., Chen, J., Makar, P., Cady-Pereira, K. E., Tam, N., and Kharol, S. K.: Satellite-derived emissions of carbon monoxide, ammonia, and nitrogen dioxide from the 2016 Horse River wildfire in the Fort McMurray area, Atmospheric Chemistry and Physics, 19, 2577-2599, 2019.

Akagi, S., Yokelson, R. J., Wiedinmyer, C., Alvarado, M., Reid, J., Karl, T., Crounse, J., and Wennberg, P.: Emission factors for open and domestic biomass burning for use in atmospheric models, Atmospheric Chemistry and Physics, 11, 4039-4072, 2011.

Alencar, A., Nepstad, D., and Moutinho, P.: Carbon emissions associated with forest fires in Brazil, Tropical deforestation and climate change, 23, 2005.

Alvarado, M., Logan, J., Mao, J., Apel, E., Riemer, D., Blake, D., Cohen, R., Min, K.-E., Perring, A., and Browne, E.: Nitrogen oxides and PAN in plumes from boreal fires during ARCTAS-B and their impact on ozone: an integrated analysis of aircraft and satellite observations, Atmospheric Chemistry and Physics, 10, 9739-9760, 2010.

Andreae, M. and Rosenfeld, D.: Aerosol–cloud–precipitation interactions. Part 1. The nature and sources of cloud-active aerosols, Earth-Science Reviews, 89, 13-41, 2008.

Andreae, M. O.: Emission of trace gases and aerosols from biomass burning–an updated assessment, Atmospheric Chemistry and Physics, 19, 8523-8546, 2019.

Andreae, M. O. and Merlet, P.: Emission of trace gases and aerosols from biomass burning, Global biogeochemical cycles, 15, 955-966, 2001.

Arellano Jr, A. F. and Hess, P. G.: Sensitivity of top‐down estimates of CO sources to GCTM transport, Geophysical Research Letters, 33, 2006.

Arellano Jr, A. F., Kasibhatla, P. S., Giglio, L., van der Werf, G. R., and Randerson, J. T.: Top‐down estimates of global CO sources using MOPITT measurements, Geophysical research letters, 31, 2004.

Balshi, M. S., McGuire, A. D., Duffy, P., Flannigan, M., Kicklighter, D. W., and Melillo, J.: Vulnerability of carbon storage in North American boreal forests to wildfires during the 21st century, Global change biology, 15, 1491-1510, 2009.

Barré, J., Gaubert, B., Arellano, A. F., Worden, H. M., Edwards, D. P., Deeter, M. N., Anderson, J. L., Raeder, K., Collins, N., and Tilmes, S.: Assessing the impacts of assimilating IASI and MOPITT CO retrievals using CESM‐CAM‐chem and DART, Journal of Geophysical Research: Atmospheres, 120, 10,501-510,529, 2015.

Beck, H. E., Zimmermann, N. E., McVicar, T. R., Vergopolan, N., Berg, A., and Wood, E. F.: Present and future Köppen-Geiger climate classification maps at 1-km resolution, Scientific data, 5, 1-12, 2018.

Bian, H., Chin, M., Kawa, S., Duncan, B., Arellano, A., and Kasibhatla, P.: Sensitivity of global CO simulations to uncertainties in biomass burning sources, Journal of Geophysical Research: Atmospheres, 112, 2007.

Boschetti, L., Roy, D. P., Justice, C. O., and Humber, M. L.: MODIS–Landsat fusion for large area 30 m burned area mapping, Remote Sensing of Environment, 161, 27-42, 2015.

Boschetti, L., Roy, D. P., Giglio, L., Huang, H., Zubkova, M., and Humber, M. L.: Global validation of the collection 6 MODIS burned area product, Remote sensing of environment, 235, 111490, 2019.

Boucher, O., Randall, D., Artaxo, P., et al.: Clouds and aerosols, Climate change 2013: The physical science basis, Contribution of working group I to the fifth assessment report of the intergovernmental panel on climate change, Cambridge University Press, 571-657, 2013.

Brando, P. M., Soares-Filho, B., Rodrigues, L., Assunção, A., Morton, D., Tuchschneider, D., Fernandes, E., Macedo, M., Oliveira, U., and Coe, M.: The gathering firestorm in southern Amazonia, Science Advances, 6, eaay1632, 2020.

Brown-Steiner, B., Selin, N. E., Prinn, R., Tilmes, S., Emmons, L., Lamarque, J.-F., and Cameron-Smith, P.: Evaluating simplified chemical mechanisms within present-day simulations of the Community Earth System Model version 1.2 with CAM4 (CESM1. 2 CAM-chem): MOZART-4 vs. Reduced Hydrocarbon vs. Super-Fast chemistry, Geoscientific Model Development, 11, 4155-4174, 2018.

Carter, T. S., Heald, C. L., Jimenez, J. L., Campuzano-Jost, P., Kondo, Y., Moteki, N., Schwarz, J. P., Wiedinmyer, C., Darmenov, A. S., and da Silva, A. M.: How emissions uncertainty influences the distribution and radiative impacts of smoke from fires in North America, Atmospheric Chemistry and Physics, 20, 2073-2097, 2020.

Chen, Y., Li, Q., Randerson, J., Lyons, E., Kahn, R., Nelson, D., and Diner, D.: The sensitivity of CO and aerosol transport to the temporal and vertical distribution of North American boreal fire emissions, Atmospheric Chemistry and Physics, 9, 6559-6580, 2009.

Christian, T. J., Kleiss, B., Yokelson, R. J., Holzinger, R., Crutzen, P. J., Hao, W. M., Saharjo, B. H., and Ward, D. E.: Comprehensive laboratory measurements of biomass‐burning emissions: 1. Emissions from Indonesian, African, and other fuels, Journal of Geophysical Research: Atmospheres, 108(D23), 2003.

Christian, K., Wang, J., Ge, C., Peterson, D., Hyer, E., Yorks, J., and McGill, M.: Radiative forcing and stratospheric warming of pyrocumulonimbus smoke aerosols: First modeling results with multisensor (EPIC, CALIPSO, and CATS) views from space, Geophysical Research Letters, 46, 10061-10071, 2019.
Cochrane, M. A.: Fire science for rainforests, Nature, 421, 913-919, 2003.
Cochrane, M. A. and Laurance, W. F.: Fire as a large-scale edge effect in Amazonian forests, Journal of Tropical Ecology, 18, 311-325, 2002.
Danabasoglu, G., Lamarque, J. F., Bacmeister, J., Bailey, D., DuVivier, A., Edwards, J., Emmons, L., Fasullo, J., Garcia, R., and Gettelman, A.: The community earth system model version 2 (CESM2), Journal of Advances in Modeling Earth Systems, 12, e2019MS001916, 2020.
Darmenov, A., da Silvia, A., and Koster, R.: The Quick Fire Emissions Dataset (QFED): Documentation of Versions 2.1, 2.2 and 2.4. Volume 38; Technical Report Series on Global Modeling and Data Assimilation, 2015.
Deeter, M., Francis, G., Gille, J., Mao, D., Martínez-Alonso, S., Worden, H., Ziskin, D., Drummond, J., Commane, R., and Diskin, G.: The MOPITT Version 9 CO product: sampling enhancements and validation, Atmospheric Measurement Techniques, 15, 2325-2344, 2022.
Ding, K., Huang, X., Ding, A., Wang, M., Su, H., Kerminen, V.-M., Petäjä, T., Tan, Z., Wang, Z., and Zhou, D.: Aerosol-boundary-layer-monsoon interactions amplify semi-direct effect of biomass smoke on low cloud formation in Southeast Asia, Nature communications, 12, 1-9, 2021.
Duncan, B. N., Martin, R. V., Staudt, A. C., Yevich, R., and Logan, J. A.: Interannual and seasonal variability of biomass burning emissions constrained by satellite observations, Journal of Geophysical Research: Atmospheres, 108, ACH 1-1-ACH 1-22, 2003.
Emmons, L.: Coauthors, 2020: The chemistry mechanism in the community earth system model version 2 (CESM2), J. Adv. Model. Earth Syst, 12, e2019MS001882, 2020.
Ferek, R. J., Reid, J. S., Hobbs, P. V., Blake, D. R., and Liousse, C.: Emission factors of hydrocarbons, halocarbons, trace gases and particles from biomass burning in Brazil, Journal of Geophysical Research: Atmospheres, 103, 32107-32118, 1998.
Ferrada, G. A., Zhou, M., Wang, J., Lyapustin, A., Wang, Y., Freitas, S. R., and Carmichael, G. R.: Introducing the VIIRS-based Fire Emission Inventory version 0 (VFEIv0), Geoscientific Model Development, 15, 8085-8109, 2022.
Firms, L.: Collection 6 NRT hotspot/active fire detections MCD14DL, En ligne: https://earthdata. nasa. gov/firms (visité le 21 June 2017), 2017.
Freitas, S., Longo, K., and Andreae, M.: Impact of including the plume rise of vegetation fires in numerical simulations of associated atmospheric pollutants, Geophysical Research Letters, 33, 2006.
Freitas, S., Longo, K., Trentmann, J., and Latham, D.: Sensitivity of 1-D smoke plume rise models to the inclusion of environmental wind drag, Atmospheric Chemistry and Physics, 10, 585-594, 2010.
GMAO: MERRA‐2 inst3_3d_asm_Np: 3d, 3‐hourly, instantaneous, pressure‐level, assimilation, assimilated meteorological fields V5. 12.4, 2015.
Gibson, C. M., Chasmer, L. E., Thompson, D. K., Quinton, W. L., Flannigan, M. D., and Olefeldt, D.: Wildfire as a major driver of recent permafrost thaw in boreal peatlands, Nature communications, 9, 3041, 2018.
Giglio, L., Randerson, J. T., and van der Werf, G. R.: Analysis of daily, monthly, and annual burned area using the fourth‐generation global fire emissions database (GFED4), Journal of Geophysical Research: Biogeosciences, 118, 317-328, 2013.

Guenther, A., Jiang, X., Heald, C. L., Sakulyanontvittaya, T., Duhl, T. a., Emmons, L., and Wang, X.: The Model of Emissions of Gases and Aerosols from Nature version 2.1 (MEGAN2. 1): an extended and updated framework for modeling biogenic emissions, Geoscientific Model Development, 5, 1471-1492, 2012.

He, J. and Zhang, Y.: Improvement and further development in CESM/CAM5: gas-phase chemistry and inorganic aerosol treatments, Atmospheric Chemistry and Physics, 14, 9171-9200, 2014.

He, J., Zhang, Y., Tilmes, S., Emmons, L., Lamarque, J.-F., Glotfelty, T., Hodzic, A., and Vitt, F.: CESM/CAM5 improvement and application: comparison and evaluation of updated CB05_GE and MOZART-4 gas-phase mechanisms and associated impacts on global air quality and climate, Geoscientific Model Development, 8, 3999-4025, 2015.

Hoelzemann, J. J., Schultz, M. G., Brasseur, G. P., Granier, C., and Simon, M.: Global Wildland Fire Emission Model (GWEM): Evaluating the use of global area burnt satellite data, Journal of Geophysical Research: Atmospheres, 109, 2004.

Hoesly, R. M., Smith, S. J., Feng, L., Klimont, Z., Janssens-Maenhout, G., Pitkanen, T., Seibert, J. J., Vu, L., Andres, R. J., and Bolt, R. M.: Historical (1750–2014) anthropogenic emissions of reactive gases and aerosols from the Community Emissions Data System (CEDS), Geoscientific Model Development, 11, 369-408, 2018.

Holben, B. N., Eck, T. F., Slutsker, I. a., Tanre, D., Buis, J., Setzer, A., Vermote, E., Reagan, J. A., Kaufman, Y., and Nakajima, T.: AERONET—A federated instrument network and data archive for aerosol characterization, Remote sensing of environment, 66, 1-16, 1998.

Huang, X., Ding, K., Liu, J., Wang, Z., Tang, R., Xue, L., Wang, H., Zhang, Q., Tan, Z.-M., Fu, C., Davis, S. J., Andreae, M. O., and Ding, A.: Smoke-weather interaction affects extreme wildfires in diverse coastal regions, Science, 379, 457-461, doi:10.1126/science.add9843, 2023.

Ichoku, C. and Ellison, L.: Global top-down smoke-aerosol emissions estimation using satellite fire radiative power measurements, Atmospheric Chemistry and Physics, 14, 6643-6667, 2014.

Jiang, Y., Yang, X.-Q., Liu, X., Qian, Y., Zhang, K., Wang, M., Li, F., Wang, Y., and Lu, Z.: Impacts of wildfire aerosols on global energy budget and climate: The role of climate feedbacks, Journal of Climate, 33, 3351-3366, 2020.

Junghenn Noyes, K. T., Kahn, R. A., Limbacher, J. A., and Li, Z.: Canadian and Alaskan wildfire smoke particle properties, their evolution, and controlling factors, from satellite observations, Atmospheric Chemistry and Physics, 22, 10267-10290, 2022.

Kaiser, J., Flemming, J., Schultz, M., Suttie, M., and Wooster, M.: The MACC global fire assimilation system: First emission products (GFASv0), Tech. Memo. 596, ECMWF, Reading, UK, 2009.

Kaiser, J., Heil, A., Andreae, M., Benedetti, A., Chubarova, N., Jones, L., Morcrette, J.-J., Razinger, M., Schultz, M., and Suttie, M.: Biomass burning emissions estimated with a global fire assimilation system based on observed fire radiative power, Biogeosciences, 9, 527-554, 2012.

Kasischke, E. S. and Bruhwiler, L. P.: Emissions of carbon dioxide, carbon monoxide, and methane from boreal forest fires in 1998, Journal of Geophysical Research: Atmospheres, 107, FFR 2-1-FFR 2-14, 2002.

Kiely, L., Spracklen, D., Arnold, S., Papargyropoulou, E., Conibear, L., Wiedinmyer, C., Knote, C., and Adrianto, H.: Assessing costs of Indonesian fires and the benefits of restoring peatland, Nature communications, 12, 7044, 2021.

Knorr, W., Dentener, F., Hantson, S., Jiang, L., Klimont, Z., and Arneth, A.: Air quality impacts of European wildfire emissions in a changing climate, Atmospheric Chemistry and Physics, 16, 5685-5703, 2016.

Lamarque, J.-F., Emmons, L., Hess, P., Kinnison, D. E., Tilmes, S., Vitt, F., Heald, C., Holland, E. A., Lauritzen, P., and Neu, J.: CAM-chem: Description and evaluation of interactive atmospheric chemistry in the Community Earth System Model, Geoscientific Model Development, 5, 369-411, 2012.

Lin, C., Cohen, J. B., Wang, S., and Lan, R.: Application of a combined standard deviation and mean based approach to MOPITT CO column data, and resulting improved representation of biomass burning and urban air pollution sources, Remote Sensing of Environment, 241, 111720, 2020a.

Lin, C., Cohen, J. B., Wang, S., Lan, R., and Deng, W.: A new perspective on the spatial, temporal, and vertical distribution of biomass burning: quantifying a significant increase in CO emissions, Environmental Research Letters, 15, 104091, 2020b.

Liousse, C., Guillaume, B., Grégoire, J.-M., Mallet, M., Galy, C., Pont, V., Akpo, A., Bedou, M., Castéra, P., and Dungall, L.: Updated African biomass burning emission inventories in the framework of the AMMA-IDAF program, with an evaluation of combustion aerosols, Atmospheric Chemistry and Physics, 10, 9631-9646, 2010.

Liu, L., Cheng, Y., Wang, S., Wei, C., Pöhlker, M. L., Pöhlker, C., Artaxo, P., Shrivastava, M., Andreae, M. O., and Pöschl, U.: Impact of biomass burning aerosols on radiation, clouds, and precipitation over the Amazon: relative importance of aerosol–cloud and aerosol–radiation interactions, Atmospheric Chemistry and Physics, 20, 13283-13301, 2020a.

Liu, T., Mickley, L. J., Marlier, M. E., DeFries, R. S., Khan, M. F., Latif, M. T., and Karambelas, A.: Diagnosing spatial biases and uncertainties in global fire emissions inventories: Indonesia as regional case study, Remote Sensing of Environment, 237, 111557, 2020b.

Liu, X., Ma, P.-L., Wang, H., Tilmes, S., Singh, B., Easter, R., Ghan, S., and Rasch, P.: Description and evaluation of a new four-mode version of the Modal Aerosol Module (MAM4) within version 5.3 of the Community Atmosphere Model, Geoscientific Model Development, 9, 505-522, 2016.

Liu, Y., Zhang, K., Qian, Y., Wang, Y., Zou, Y., Song, Y., Wan, H., Liu, X., and Yang, X.-Q.: Investigation of short-term effective radiative forcing of fire aerosols over North America using nudged hindcast ensembles, Atmospheric Chemistry and Physics, 18, 31-47, 2018.

McMeeking, G. R., Kreidenweis, S. M., Baker, S., Carrico, C. M., Chow, J. C., Collett Jr, J. L., Hao, W. M., Holden, A. S., Kirchstetter, T. W., and Malm, W. C.: Emissions of trace gases and aerosols during the open combustion of biomass in the laboratory, Journal of Geophysical Research: Atmospheres, 114, 2009.

Mieville, A., Granier, C., Liousse, C., Guillaume, B., Mouillot, F., Lamarque, J.-F., Grégoire, J.-M., and Pétron, G.: Emissions of gases and particles from biomass burning during the 20th century using satellite data and an historical reconstruction, Atmospheric Environment, 44, 1469-1477, 2010.

Neu, J. and Prather, M.: Toward a more physical representation of precipitation scavenging in global chemistry models: cloud overlap and ice physics and their impact on tropospheric ozone, Atmospheric Chemistry and Physics, 12, 3289-3310, 2012.

Olson, D. M., Dinerstein, E., Wikramanayake, E. D., Burgess, N. D., Powell, G. V., Underwood, E. C., D'amico, J. A., Itoua, I., Strand, H. E., and Morrison, J. C.: Terrestrial Ecoregions of the World: A New Map of Life on EarthA new global map of terrestrial ecoregions provides an innovative tool for conserving biodiversity, BioScience, 51, 933-938, 2001.

Page, S. E., Siegert, F., Rieley, J. O., Boehm, H.-D. V., Jaya, A., and Limin, S.: The amount of carbon released from peat and forest fires in Indonesia during 1997, Nature, 420, 61-65, 2002.

Pan, X., Ichoku, C., Chin, M., Bian, H., Darmenov, A., Colarco, P., Ellison, L., Kucsera, T., da Silva, A., and Wang, J.: Six global biomass burning emission datasets: intercomparison and application in one global aerosol model, Atmospheric Chemistry and Physics, 20, 969-994, 2020.

Paton-Walsh, C., Emmons, L. K., and Wiedinmyer, C.: Australia's Black Saturday fires–Comparison of techniques for estimating emissions from vegetation fires, Atmospheric Environment, 60, 262-270, 2012.

Paton‐Walsh, C., Deutscher, N. M., Griffith, D., Forgan, B., Wilson, S., Jones, N., and Edwards, D.: Trace gas emissions from savanna fires in northern Australia, Journal of Geophysical Research: Atmospheres, 115, 2010.

Platnick, S., King, M., Meyer, K., Wind, G., Amarasinghe, N., Marchant, B., Arnold, G., Zhang, Z., Hubanks, P., and Ridgway, B.: MODIS atmosphere L3 monthly product, NASA MODIS Adaptive processing system, goddard space flight center, USA, 20, 2015.

Pokhrel, R. P., Gordon, J., Fiddler, M. N., Bililign, S.: Impact of combustion conditions on physical and morphological properties of biomass burning aerosol, Aerosol Science and Technology, 55(1), 80-91, 2021.

Ramnarine, E., Kodros, J. K., Hodshire, A. L., Lonsdale, C. R., Alvarado, M. J., and Pierce, J. R.: Effects of near-source coagulation of biomass burning aerosols on global predictions of aerosol size distributions and implications for aerosol radiative effects, Atmospheric Chemistry and Physics, 19, 6561-6577, 2019.

Randerson, J. T., van der Werf, G. R., Giglio, L., Collztz, G. J., and Kasibhatla, P. S.: Global Fire Emission Database, Version 4.1 (GFEDv4). ORNLDAAC, Oak Ridge, Tennessee, USA, 2018. https://doi.org/10.3334/ORNLDAAC/1293

Reid, W. V. and Mooney, H. A.: The Millennium Ecosystem Assessment: testing the limits of interdisciplinary and multi-scale science, Current Opinion in Environmental Sustainability, 19, 40-46, 2016.

Reid, W. V., Mooney, H. A., Cropper, A., Capistrano, D., Carpenter, S. R., Chopra, K., Dasgupta, P., Dietz, T., Duraiappah, A. K., and Hassan, R.: Ecosystems and human well-being-Synthesis: A report of the Millennium Ecosystem Assessment, Island Press, 2005.

Roy, D. P., Boschetti, L., Justice, C., and Ju, J.: The collection 5 MODIS burned area product—Global evaluation by comparison with the MODIS active fire product, Remote sensing of Environment, 112, 3690-3707, 2008.

Spracklen, D., Jimenez, J., Carslaw, K., Worsnop, D., Evans, M., Mann, G., Zhang, Q., Canagaratna, M., Allan, J., and Coe, H.: Aerosol mass spectrometer constraint on the global secondary organic aerosol budget, Atmospheric Chemistry and Physics, 11, 12109-12136, 2011.

Stockwell, T., Zhao, J., Greenfield, T., Li, J., Livingston, M., and Meng, Y.: Estimating under‐and over‐reporting of drinking in national surveys of alcohol consumption: identification of consistent biases across four English‐speaking countries, Addiction, 111, 1203-1213, 2016.

Tilmes, S., Hodzic, A., Emmons, L., Mills, M., Gettelman, A., Kinnison, D. E., Park, M., Lamarque, J. F., Vitt, F., and Shrivastava, M.: Climate forcing and trends of organic aerosols in the Community Earth System Model (CESM2), Journal of Advances in Modeling Earth Systems, 11, 4323-4351, 2019.

Urbanski, S., Hao, W., and Nordgren, B.: The wildland fire emission inventory: western United States emission estimates and an evaluation of uncertainty, Atmospheric Chemistry and Physics, 11, 12973-13000, 2011.

van der Werf, G., Randerson, J., Giglio, L., Collatz, J., Kasibhatla, P., Morton, D., and DeFries, R.: The improved Global Fire Emissions Database (GFED) version 3: contribution of savanna, forest, deforestation, and peat fires to the global fire emissions budget, EGU General Assembly Conference Abstracts, 2010a.

van der Werf, G. R., Randerson, J. T., Giglio, L., Collatz, G. J., Kasibhatla, P. S., and Arellano Jr, A. F.: Interannual variability in global biomass burning emissions from 1997 to 2004, Atmospheric Chemistry and Physics, 6, 3423-3441, 2006.

van der Werf, G. R., Randerson, J. T., Giglio, L., Collatz, G., Mu, M., Kasibhatla, P. S., Morton, D. C., DeFries, R., Jin, Y. v., and van Leeuwen, T. T.: Global fire emissions and the contribution of deforestation, savanna, forest, agricultural, and peat fires (1997–2009), Atmospheric chemistry and physics, 10, 11707-11735, 2010b.

van der Werf, G. R., Randerson, J. T., Giglio, L., van Leeuwen, T. T., Chen, Y., Rogers, B. M., Mu, M., van Marle, M. J., Morton, D. C., and Collatz, G. J.: Global fire emissions estimates during 1997–2016, Earth System Science Data, 9, 697-720, 2017.

Vetrita, Y., Cochrane, M. A., Priyatna, M., Sukowati, K. A., and Khomarudin, M. R.: Evaluating accuracy of four MODIS-derived burned area products for tropical peatland and non-peatland fires, Environmental Research Letters, 16, 035015, 2021.

Warner, J. X., Gille, J. C., Edwards, D. P., Ziskin, D. C., Smith, M. W., Bailey, P. L., and Rokke, L.: Cloud detection and clearing for the Earth Observing System Terra satellite Measurements of Pollution in the Troposphere (MOPITT) experiment, Applied Optics, 40, 1269-1284, 2001.

Webb, M. J., Andrews, T., Bodas-Salcedo, A., Bony, S., Bretherton, C. S., Chadwick, R., Chepfer, H., Douville, H., Good, P., and Kay, J. E.: The cloud feedback model intercomparison project (CFMIP) contribution to CMIP6, Geoscientific Model Development, 10, 359-384, 2017.

Westerling, A. L. and Bryant, B.: Climate change and wildfire in California, Climatic Change, 87, 231-249, 2008.

Westerling, A. L., Hidalgo, H. G., Cayan, D. R., and Swetnam, T. W.: Warming and earlier spring increase western US forest wildfire activity, science, 313, 940-943, 2006.

Wiedinmyer, C., Akagi, S., Yokelson, R. J., Emmons, L., Al-Saadi, J., Orlando, J., and Soja, A.: The Fire INventory from NCAR (FINN): A high resolution global model to estimate the emissions from open burning, Geoscientific Model Development, 4, 625-641, 2011.

Wiedinmyer, C., Quayle, B., Geron, C., Belote, A., McKenzie, D., Zhang, X., O'Neill, S., and Wynne, K. K.: Estimating emissions from fires in North America for air quality modeling, Atmospheric Environment, 40, 3419-3432, 2006.

Williams, J. E., van Weele, M., van Velthoven, P. F., Scheele, M. P., Liousse, C., and van Der Werf, G. R.: The impact of uncertainties in African biomass burning emission estimates on modeling global air quality, long range transport and tropospheric chemical lifetimes, Atmosphere, 3, 132-163, 2012.

Yang, Y., Smith, S. J., Wang, H., Mills, C. M., and Rasch, P. J.: Variability, timescales, and nonlinearity in climate responses to black carbon emissions, Atmospheric Chemistry and Physics, 19, 2405-2420, 2019.

Yokelson, R. J., Susott, R., Ward, D. E., Reardon, J., and Griffith, D. W. T.: Emissions from smoldering combustion of biomass measured by open-path Fourier transform infrared spectroscopy, Journal of Geophysical Research: Atmospheres, 102(D15), 18865-18877, 1997.

Yu, P., Toon, O. B., Bardeen, C. G., Zhu, Y., Rosenlof, K. H., Portmann, R. W., Thornberry, T. D., Gao, R.-S., Davis, S. M., and Wolf, E. T.: Black carbon lofts wildfire smoke high into the stratosphere to form a persistent plume, Science, 365, 587-590, 2019.

Zhang, Y., Li, Z., Chen, Y., de Leeuw, G., Zhang, C., Xie, Y., and Li, K.: Improved inversion of aerosol components in the atmospheric column from remote sensing data, Atmospheric Chemistry and Physics, 20, 12795-12811, 2020.

Table 1. Brief introduction of four BB inventories

Inventory	"Bottom-up"		"Top-down"	
	FINN1.5	GFED4s	QFED2.5	VFEI0
Temporal range	2002- (NRT) [a]	1997-2022[b]	2000- (NRT) [a]	2012- (NRT) [a]
Spatio-temporal resolution	1km, daily	0.25°, monthly (daily fraction)	0.1°, daily (0.25° × 0.375°, NRT [a])	500m, daily
Primary satellite fire input	MCD14DL C5 active fire area (1km)	MCD64A1 C5.1 burned area (500m)	MOD14/MYD14 C6 FRP (1km)	VNP14IMG FRP (1km)
Statistical boosts/Adjustion	Smooth assumption in tropics [c]	Small fire boost (MOD14A1/MYD14A1)	Cloud-gap adjusted FRP density	
Primary land use/land cover (LULC)	MCD12Q1 (IGBP), 2005	MCD12Q1 (UMD), 2001-2012	IGBP-INPE	MCD12C1(IGBP) + The Köppen Climate Classification
Peatland fire	×	Olson et al. (2001)	×	Ferrada et al. (2022)
Conversion to dry matter	Hoelzemann et al. (2004)	CASA biogeochemical model (van der Werf et al., 2010)	QFED FRP vs GFED2 dry matter global calibration	VFEI FRP vs GFED3.1 dry matter global calibration
Emission factors	Akagi et al. (2011), Andreae and Merlet (2001)	Akagi et al. (2011) + updates from Andreae et al. (2013)	Andreae and Merlet (2001), Akagi et al. (2011) [d]	Akagi et al. (2019)
Speciation	41 species	27 species	17 species	46 species
References	Wiedinmyer et al. (2011)	van der Werf et al. (2017)	Darmenov and da Silva (2015)	Ferrada et al. (2022)

a: NRT = near real time; b: 2017-2022 are beta version releases;

c: In equatorial region (30°N-30°S), each detected fire will be counted as 2-day, assuming the second day's fire will continue to be half the size of the previous day;

d: Particulate matter-related emissions from biomass burning (e.g. BC, OC, NH_3, SO_2, and $PM_{2.5}$) were corrected from emission factors based on MODIS AOD.

Table 2. CO and OC emission factors used in the four biomass burning emission inventories.

	Emission factors across inventories and vegetation types (g species per kg dry matter)							
Types	CO				OC			
	FINN1.5	GFED4s	QFED2.5	VFEI0	FINN1.5	GFED4s	QFED2.5	VFEI0
Temperate forest	108[Ak]	88[Ak]	107[AM]	113[An]	6.97[AR]	9.6[AM]	41.09*	10.9[An]
Boreal forest	118[Ak]	127[Ak]	107[AM]	121[An]	7.31[Mc]	9.6[AM]	41.09*	5.9.[An]
Savanna and Grass, shrub	59[Ak]/68[Ak]	63[Ak]	65[AM]	69[An]	2.6[Ak]/6.61[Mc]	2.62[Ak]	6.12*	3[An]
Tropical forest	92[Ak]	93[Ak]	104[AM]	104[An]	4.77[Ak]	4.71[Ak]	13*	4.4[An]
Agricultural	111[Ak]	102[Ak]	/	76[An]	3.3[AM]	2.3[Ak]	/	4.9[An]
Peatlands	/	210[#]	/	260[An]	/	6.02[#]	/	14.2[An]

Ak: Akagi et al. (2011); AM: Andreae and Merlet (2001); An: Andreae (2019); AR: Andreae and Rosenfeld (2008); Mc: McMeeking et al. (2009)

*: QFED2.5 PM-related emission factors are obtained by multiplying the base EF multiplied by its biome-specific enhancement factor

#: Emission factors for peatland is the average of lab measurements of Yokelson et al. (1997) and Christian et al. (2003)

Table 3. Comparison of CESM-CAM6 simulated CO column averages and satellite retrieved CO column averages during the fire season.

		Satellite	CESM2-CAM6			
Regions	Fire-Season	MOPITT	FINN1.5	GFED4s	QFED2.5	VFEI0
EQAS	Jan.-Apr.	1.88	1.66	*1.69*	1.61	1.47
BONA	Apr.-Aug.	2.03	1.29	*1.47*	1.30	1.32
SEAS	Feb.-Apr.	2.40	*2.10*	1.94	1.89	1.95
SHAF	May.-Nov.	2.31	1.75	2.04	1.99	*2.19*
NHAF	Jan.-May.	2.66	1.96	2.02	2.05	*2.10*
BOAS	Mar.-Nov.	2.05	1.31	*1.42*	1.33	1.34
SHSA	July.-Dec.	1.77	*1.75*	*1.80*	*1.76*	*1.80*

1053 **Table 4. Same as Table 3 but for AOD**

	Satellite	CESM2-CAM6			
Regions	MODIS	FINN1.5	GFED4s	QFED2.5	VFEI0
EQAS	0.23	*0.22*	*0.25*	*0.23*	*0.21*
BONA	0.13	0.07	*0.12*	*0.11*	0.07
SEAS	0.30	0.35	*0.30*	0.36	*0.30*
SHAF	0.33	*0.31*	*0.37*	0.53	*0.40*
NHAF	0.32	*0.53*	0.54	0.61	0.55
BOAS	0.15	0.11	*0.13*	*0.16*	0.11
SHSA	0.14	0.30	0.31	0.34	*0.29*

1054

1055

1056

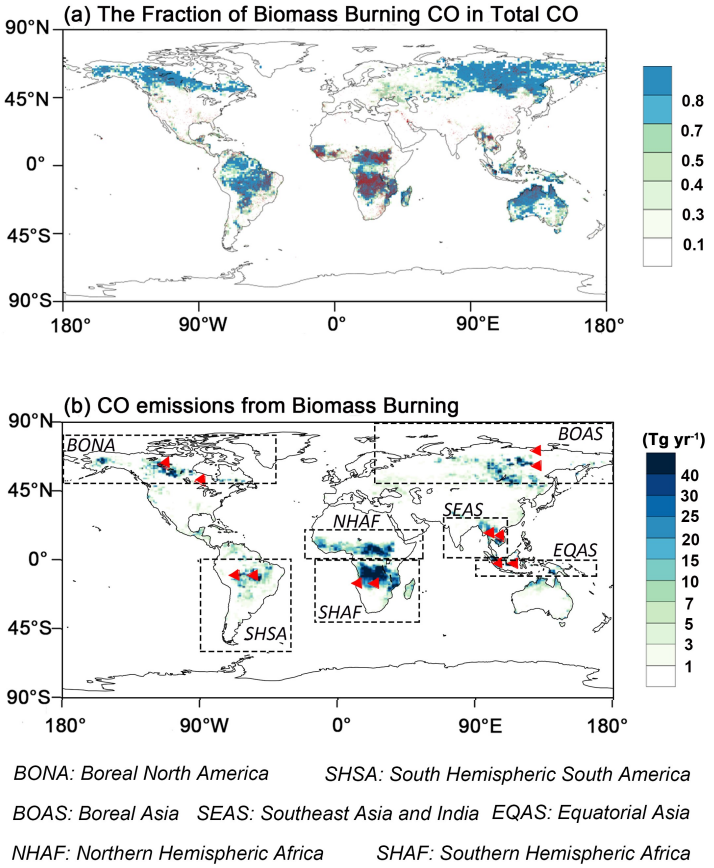

Figure 1. (a) The fraction of BB CO emissions to the sum of anthropogenic and BB CO emissions (CO_BB/CO_Total) during 2013-2016 and (b) the spatial distribution of CO emissions (FINN1.5 was used as an example). The red dots in Fig. 1(a) are the fire points from the MCD14DL satellite product. In Fig. 1(b), seven regions with high BB emissions taken from those applied by van der Werf et al. (2006, 2010) are marked with black boxes, and the red triangles represent 12 AERONET stations. In this study, seven major BB regions includes Boreal North America (BONA), Boreal Asia (BOAS), Southeast Asia (SEAS), Equatorial Asia (EQAS), North Hemisphere Africa (NHAF), South Hemisphere Africa (SHAF), and South Hemisphere South America (SHSA).

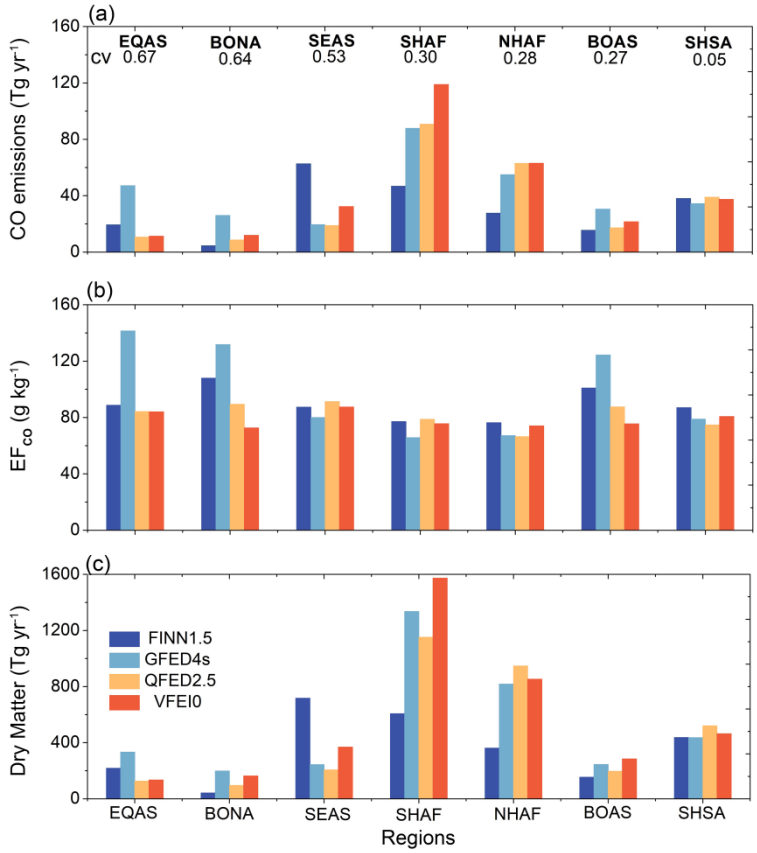

1070

1071 **Figure 2.** (a) Average annual CO emissions of four biomass burning emission inventories across seven
1072 major BB regions during 2013-2016. The cv, defined as the ratio of the standard deviation to the mean,
1073 is the coefficient of variation among the emissions of four datasets. (b) and (c) are the same as (a), but
1074 for the emission factor of CO (EF_{CO}) and Dry Matter.

1075

1076

1077

1078

1079

1080

1081

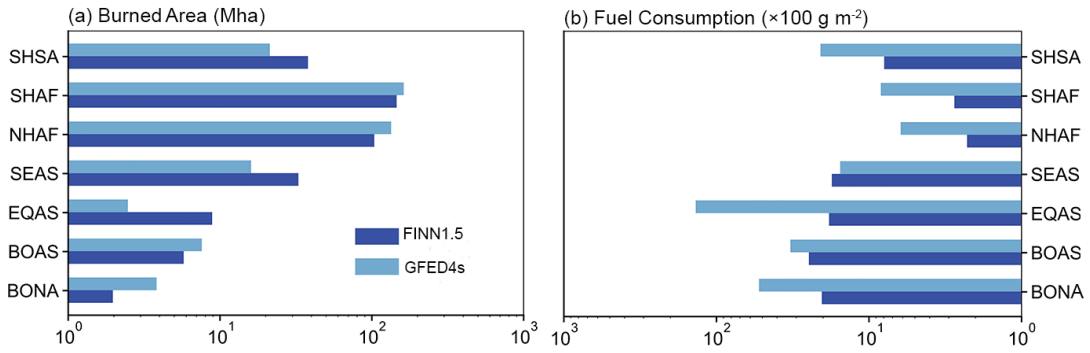

Figure 3. Annual burned area (a) and fuel consumption (b) of two bottom-up datasets (FINN1.5 and GFED4s) across seven regions from 2013 to 2016.

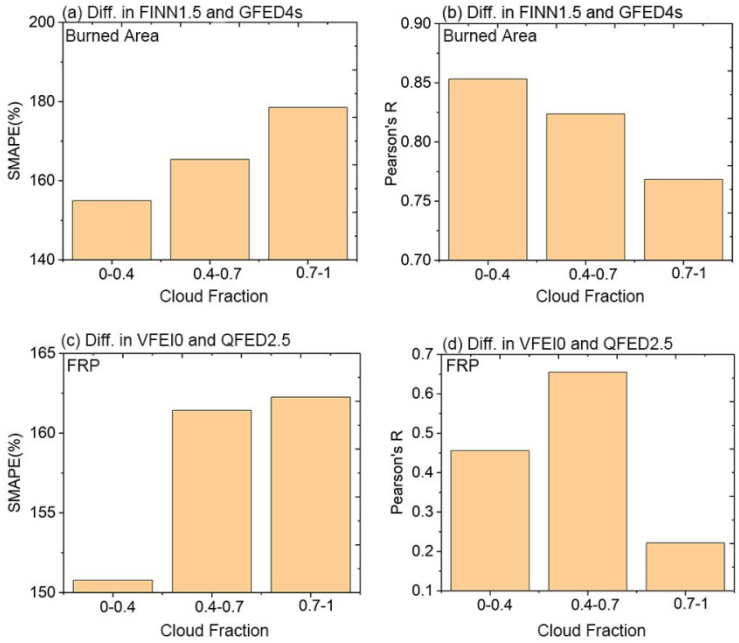

Figure 4. The differences in (a-b) burned areas and (c-d) total FRP detected by two inventories under different cloud fraction in a pilot region of BONA. These differences are quantified by two indicators: SMAPE and Pearson's R. Could fraction data is calculated from MODIS product MCD06COSP.

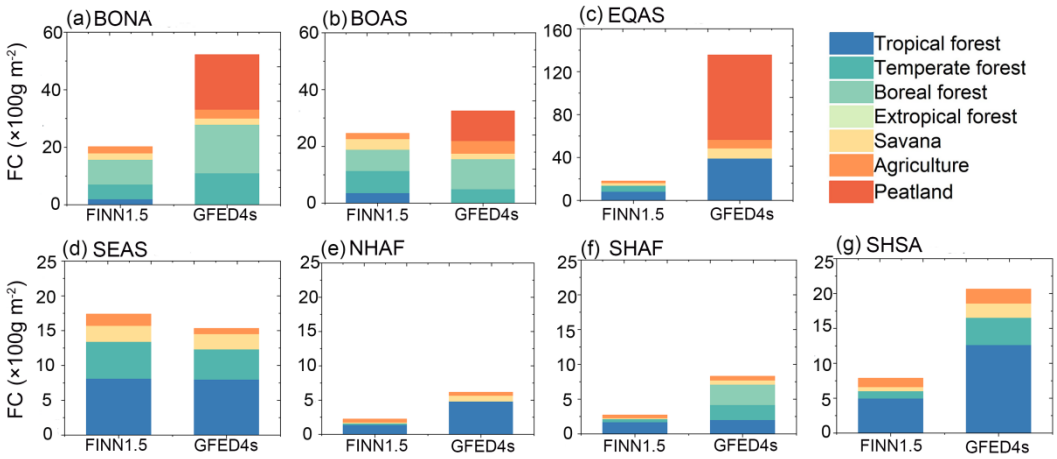

Figure 5. Annual average fuel consumption of two bottom-up datasets (FINN1.5 and GFED4s) across seven regions from 2013 to 2016. The contributions of the seven biomes are shown in different colors.

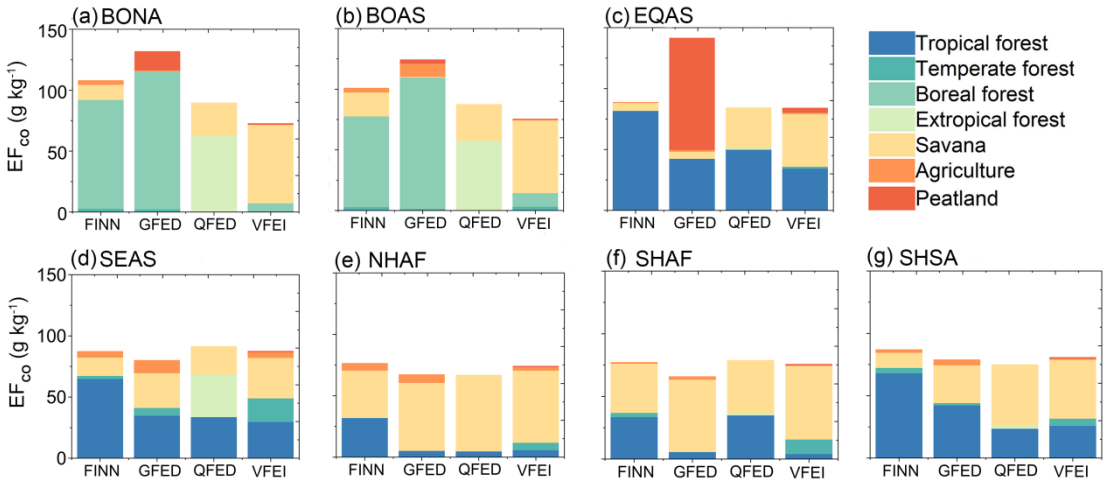

Figure 6. Regional comprehensive emission factors for four datasets (FINN1.5, GFED4s, QFED2.5, and VFEI0) in seven regions from 2013 to 2016. The contributions of the seven biomes are shown in different colors.

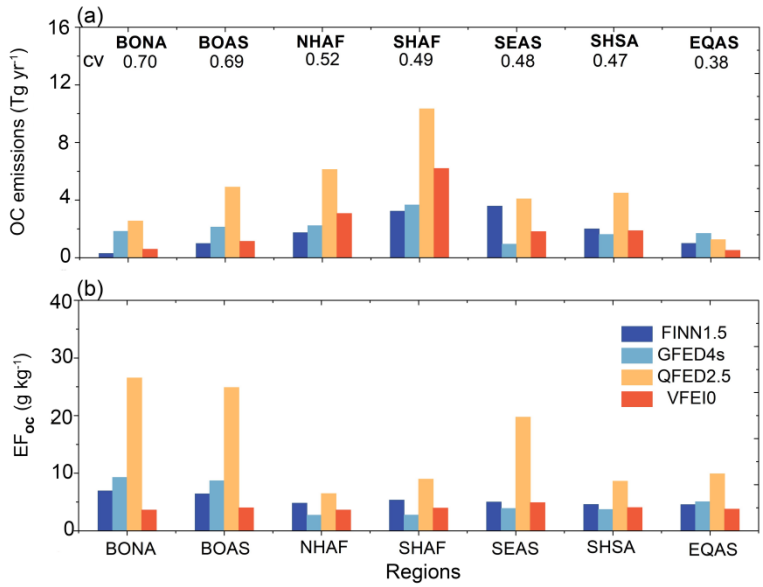

Figure 7. (a) Average annual OC emissions of four biomass burning emissions inventories across seven major BB regions during 2013-2016. The cv, defined as the ratio of the standard deviation to the mean, is the coefficient of variation among the emissions of four datasets. (b) is the same as (a) but for the emission factor of OC (EF_{oc}).

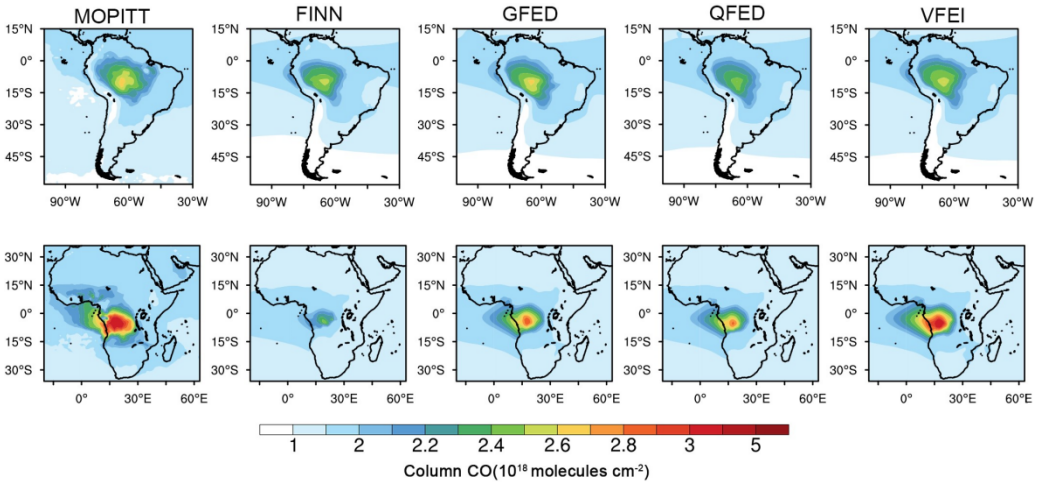

Figure 8. Spatial distribution of CO column burdens from MOPITT and CESM2-CAM6 simulations during the fire season (Table 3). The text above each plot identifies the name of the satellite inversion dataset or emission inventory dataset applied by the model, namely FINN1.5, GFED4s, QFED2.5, and VFEI0.

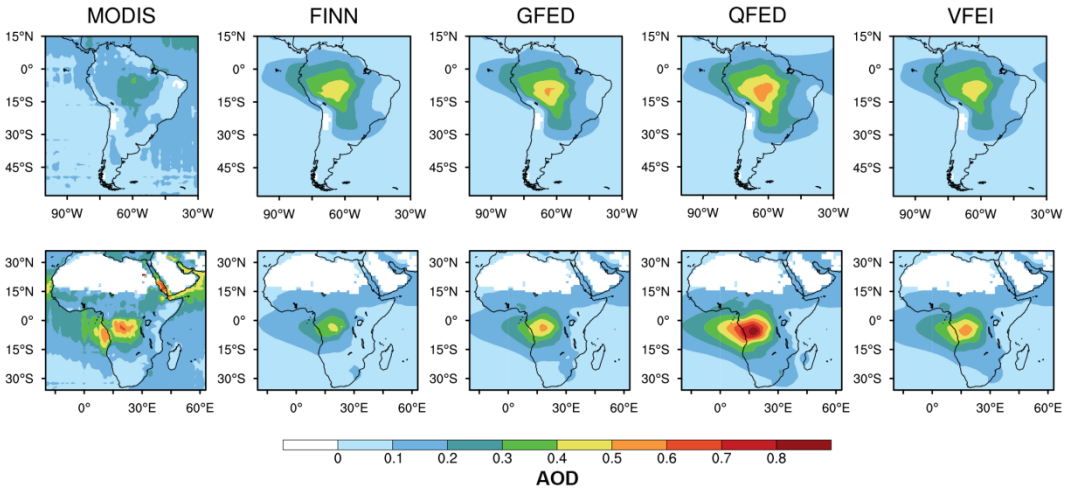

Figure 9. The same as figure 8 but for AOD.

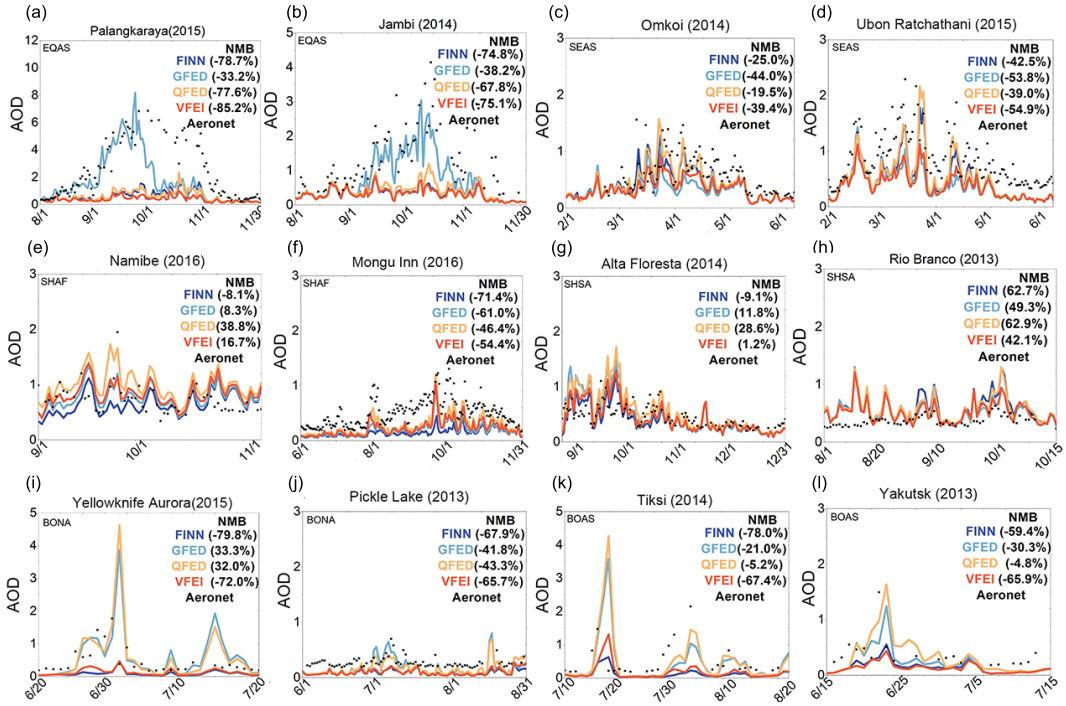

Figure 10. Comparison between AOD simulated by CESM2-CAM6 using the four datasets (FINN1.5, GFED4s, QFED2.5, and VFEI0) and AERONET ground-based observations during fire seasons. These AERONET sites are: (a) Palangkaraya (2.2°S, 113.9°E), (b) Jambi (1.6°S, 103.6°E), (c) Omkoi (17.8°N, 98.4°E), (d) Ubon Ratchathani (15.2°N, 104.9°E), (e) Namibe (15.2°S, 12.2°E), (f) Mongu Inn (15.3°S, 23.1°E), (g) Alta Floresta (9.9°S, 56.1°W), (h) Rio Branco (9.9°S, 67.9°W), (i) Yellowknife_Aurora (62.5°N, 114.4°W), (j) Pickle Lake (51.4°N, 90.2°W), (k) Tiksi (71.6°N, 128.9°E), (l) Yakutsk (61.7°N, 129.4°E).